Cardioprotective Effects of Erythropoietin in Rats Subjected to Ischemia–Reperfusion Injury: Assessment of Infarct Size with ^{99m}Tc-Annexin V

Tomoki Doue[1,2], Katsuichi Ohtsuki[1,2], Kazuma Ogawa[3], Masashi Ueda[4], Akihiro Azuma[1], Hideo Saji[5], Harry W. Strauss[6], and Hiroaki Matsubara[1]

[1]Department of Cardiology and Nephrology, Kyoto Prefectural University of Medicine, Kyoto, Japan; [2]Department of Medicine, Meiji University of Integrative Medicine, Nantan, Japan; [3]Division of Tracer Kinetics, Advanced Science Research Center, Kanazawa University, Kanazawa, Japan; [4]Radioisotopes Research Laboratory, Kyoto University Hospital Faculty of Medicine, Kyoto University, Kyoto, Japan; [5]Department of Patho-Functional Bioanalysis, Graduate School of Pharmaceutical Sciences, Kyoto University, Kyoto, Japan; and [6]Division of Nuclear Medicine, Department of Radiology, Memorial Sloan-Kettering Hospital, New York, New York

Administration of erythropoietin (EPO) during or immediately after myocardial ischemia can reduce subsequent myocardial apoptosis, a key phenomenon in myocardial ischemia–reperfusion injury. In this study, we assessed the effect of EPO on ^{99m}Tc-annexin V myocardial uptake and whether the accumulation of ^{99m}Tc-annexin V can predict cardiac remodeling and functional deterioration. **Methods:** Eighteen rats with left coronary artery (LCA) occlusion were randomized to receive either an intravenous injection of EPO (EPO group) or saline (nontherapy [nT] group) immediately after release of the occlusion. After 20 min of LCA occlusion and 30 min of reperfusion, the rats were injected with ^{99m}Tc-annexin V. One hour after ^{99m}Tc-annexin V injection, the LCA was reoccluded and ^{201}Tl was injected intravenously, and the rats were sacrificed 1 min later. The heart was removed and sectioned, and dual-tracer autoradiography was performed to evaluate the distribution of the area at risk (defined on the thallium autoradiograph) and the area of apoptosis (defined on the annexin autoradiograph). Adjacent histologic specimens had deoxyuridine triphosphate nick-end labeling (TUNEL) staining to confirm the presence of apoptosis and were compared with autoradiography. Another 16 rats were randomized to EPO and nT groups and underwent echocardiography immediately after release of the LCA occlusion and at 2 and 4 wk after surgery. **Results:** The areas of ^{99m}Tc-annexin V accumulation in the EPO group were smaller than those in the nT group, though the ^{201}Tl defect areas of these 2 groups were comparable (area ratio, 0.318 ± 0.038 vs. 0.843 ± 0.051, $P < 0.001$, for annexin and 24.8 ± 2.1 vs. 25.9 ± 2.6 mm^2, P = NS, for thallium). ^{99m}Tc-annexin V accumulation correlated with the density of TUNEL-positive cells (r = 0.886, $P < 0.001$). In the nT group, left ventricular end-diastolic dimension (Dd) increased from baseline at 2 wk by 34.7% ± 3.8% and remained stable at 34.9% ± 5.0% at 4 wk after coronary occlusion. In the EPO group, Dd increased by 8.5% ± 2.1% ($P < 0.01$ vs. nT at 2 wk) and 13.2% ± 2.8% ($P < 0.01$ vs. nT at 4 wk). In the nT group, the left ventricular percentage of fractional shortening decreased by 42.2% ± 3.4% and 52.9% ± 3.4% at 2 and 4 wk, respectively, whereas in the EPO group it decreased 9.0% ± 1.9% at 2 wk ($P < 0.01$ vs. nT at 2 wk) and 11.1% ± 6.7% at 4 wk ($P < 0.01$ vs. nT at 4 wk). **Conclusion:** This study demonstrated that a single treatment with EPO immediately after release of coronary ligation suppressed cardiac remodeling and functional deterioration. ^{99m}Tc-annexin V autoradiographs and TUNEL staining confirm that this change is due to a decrease in the extent of myocardial apoptosis in the ischemic/reperfused region.

Key Words: ^{99m}Tc-annexin V; erythropoietin; reperfusion; apoptosis

J Nucl Med 2008; 49:1694–1700
DOI: 10.2967/jnumed.107.050260

Restoration of oxygen to ischemic myocardium induces apoptosis in the ischemic myocytes (*1–4*). In severe, prolonged ischemia, apoptosis occurs before necrosis during the later stages of ischemic injury (*5,6*). Elimination or reduction of apoptosis would reduce the infarction and the likelihood of cardiac remodeling and of decreased left ventricular (LV) function in the infarction region and, overall, could improve prognosis.

Although erythropoietin (EPO) was developed as a hematopoietic growth factor, stimulating the production and release of red blood cells, EPO has recently been shown to protect ischemic neural and myocardial tissue (*7–9*). The hematologic and neuro/cardioprotective roles of EPO are caused by the interaction of EPO with 2 different receptors. The classic EPO receptor is responsible for the red blood cell response, whereas the interaction with the β common-receptor is responsible for the tissue protective effects (*10*). In a rat study, EPO administration dramatically reduced infarct size, resulting in improvement of long-term cardiac contractility (*11*). A single dose of EPO administered immediately after release of coronary artery ligation reduced LV remodeling

Received Feb. 17, 2008; revision accepted Jul. 1, 2008.
For correspondence or reprints contact: Tomoki Doue, Department of Medicine, Meiji University of Integrative Medicine, Hiyoshi-cho Nantan, Kyoto, 629-0392, Japan.
E-mail: doue@meiji-u.ac.jp

and dysfunction in animals undergoing experimental myocardial infarction, though the dose of EPO was far above that usually used to treat anemia (*12*). Additional studies explored various doses and intervals between ischemic injury and EPO administration to preserve cardiac function after ischemia–reperfusion injury (*12–14*). The antiapoptotic effect of EPO has been suggested as the mechanism for myocardial preservation.

Under normal circumstances, phosphatidylserine, a constituent of membrane phospholipids, is actively restricted to the inner leaflet of the plasma membrane by the action of 2 enzymes, translocase and floppase. Early in the course of apoptosis, these enzymes are inactivated. As translocase and floppase are inactivated, scramblase, an enzyme that equilibrates the membrane lipids on the inner and outer leaflet of the cell membrane, is activated. This combination of enzyme inactivation and activation results in the rapid appearance of phosphatidylserine on the outer leaflet of the cell membrane (*15*).

Annexin V, a physiologic protein with a molecular weight of about 36 kD, binds with nanomolar affinity to membrane-bound phosphatidylserine (*16,17*). Both in vitro and in vivo methods have been developed that use this characteristic of annexin V binding to identify cells in the early stages of apoptosis (*18–20*). For example, Peker et al. have used ^{99m}Tc-labeled annexin V to detect apoptosis as a result of ischemia–reperfusion injury in vivo (*21*). Other investigators have used radiolabeled annexin V to identify apoptosis in acute cardiac allograft rejection, subacute myocarditis, and acute doxorubicin cardiotoxicity (*20–22*).

This study was performed to determine the effect of a single intravenous dose of EPO on apoptotic activity and ventricular function in animals subjected to ischemia–reperfusion.

MATERIALS AND METHODS

Materials

Mutant annexin V (annexin V-117, a recombinant human annexin engineered to include a binding site for technetium, generously provided by John Tait, University of Washington) was produced by expression in *Escherichia coli* as previously described (*23*). This material preserves phosphatidylserine-binding activity equivalent to that of native annexin V. Labeling efficiency was consistently above 92%, providing a specific activity of approximately 7.4 MBq per microgram of protein using a previously described radiolabeling protocol (*23*). Under these conditions, annexin V labeling was stable for at least 4 h.

Recombinant human EPO was kindly provided by Chugai Pharmaceutical Co., Ltd.

Animal Model of Ischemia and Reperfusion Injury

Eighteen Male Wister rats (10 wk old; body weight, 305 ± 12.4 g) were anesthetized with intraperitoneally administered pentobarbital (20 mg/kg) and intubated, and anesthesia was maintained with inhalation of 2% isoflurane in 1.0 L of oxygen/min during volume-controlled ventilation. The heart was exposed through a left thoracotomy; a pledgeted 5–0 silk suture on a small, curved needle was passed through the myocardium beneath the proximal portion of the left coronary artery (LCA); and both ends of the suture were passed through a small vinyl tube to make a snare. The suture material was pulled tightly against the vinyl tube and secured by a keeper on the tube to occlude the LCA. Animals were randomized to receive either a single intravenous injection of EPO (200 units/kg in 0.3 mL of saline) or an equivalent volume of saline immediately after release of LCA occlusion (EPO group and nontherapy [nT] group, respectively, n = 9 in each). Myocardial ischemia was confirmed by ST-segment elevation on electrocardiography, regional cyanosis of the myocardial surface, and decreased regional wall motion. After a 20-min occlusion of the LCA, reperfusion was obtained by removal of the keeper and release of the snare and was confirmed by the change from cyanotic to pink in the myocardial risk area. During reperfusion, the snare was left loose on the surface of the heart for reocclusion. Approximately 55.5 MBq of ^{99m}Tc-annexin V were injected via a tail vein at 30 min after reperfusion. One hour after ^{99m}Tc-annexin V injection, the snare occluder was again pulled tightly and 0.185 MBq of ^{201}Tl was injected via a tail vein to delineate the area at risk. One minute later, the rat was euthanized by a bolus injection of 4 mL of 0.5 M KCl. The heart was excised, rapidly rinsed in saline, embedded in methylcellulose, and frozen in iced n-hexane. Serial short-axis heart sections (20- and 8-μm short-axis sections adjacent to each other) were obtained using a cryostat for autoradiography and histologic analysis, respectively. This study was approved by the institutional Animal Care Committee at Kyoto Prefectural University of Medicine.

Dual-Tracer Autoradiography

Dual-tracer autoradiography of the LV short-axis slices was performed using a bio-imaging analyzer system (BAS5000; Fuji Film). The apoptotic area was determined from the ^{99m}Tc-annexin V uptake area, and the area at risk was determined from the ^{201}Tl defect area. The first autoradiographic exposure was performed for 30 min to visualize ^{99m}Tc-annexin V. Approximately 72 h later (12 half-lives of ^{99m}Tc), the second exposure of the same heart sections was performed for 36 h to delineate the area at risk, expressed as ^{201}Tl defect area.

Data Analysis of Autoradiography

The extent and the density of the 2 radionuclides were quantitatively analyzed using the bio-imaging analyzer system. After exposure, the bioimaging plate was placed in a reader to determine the photostimulated luminescence (PSL) in each pixel (25 × 25 μm). These data were recorded for each animal and each nuclide. The accumulation of ^{99m}Tc-annexin V was assessed in 4 midventricular short-axis frozen sections. The region of decreased thallium activity seen on the autoradiograph was outlined, and the region of interest was transferred to the ^{99m}Tc-annexin V autoradiograph to evaluate ^{99m}Tc-annexin V uptake. Four background ROIs were set adjacent to the left ventricle in each autoradiograph, and the mean PSL per unit area (1 mm^2) of the 4 background ROIs was defined as background tracer uptake. The uptake values of each ROI were calculated as the background-corrected PSL per unit area (1 mm^2). The area ratio and the density ratio were defined as the indicator to evaluate the extent and intensity, respectively, of ^{99m}Tc-annexin V uptake. The area ratio calculated by dividing ^{99m}Tc-annexin V uptake area by ^{201}Tl defect area indicates the extent of the apoptotic area in the area at risk. The density ratio of ^{99m}Tc-annexin V was calculated by dividing the uptake values of the ^{99m}Tc-annexin V uptake area by that of the normally perfused area. All parameters were expressed as an average value obtained from the analysis of 4 midventricular short-axis slices in each rat.

Histopathologic Examinations

Four sets of short-axis frozen sections adjacent to the slices for autoradiography were stained with terminal deoxynucleotidyl transferase-mediated deoxyuridine triphosphate nick-end labeling (TUNEL) using a commercially available kit (in situ cell death detection kit, fluorescein isothiocyanate labeling; Roche Applied Science) according to the manufacturer's protocol. As a positive control of TUNEL staining, we used rat intestine. Rhodamine-labeled α-sarcomeric actinin (DAKO) was simultaneously used for the detection of muscular structures. Digital photographs were taken under confocal microscopy at 200× magnification. TUNEL-positive cardiomyocytes were counted in 20 randomly chosen fields within the area at risk for each section. The mean density ratio of ^{99m}Tc-annexin V was compared with the mean number of TUNEL-positive myocytes in the corresponding area of each rat. Another 2 sets of short-axis frozen sections adjacent to the slices for autoradiography were stained with hematoxylin and eosin and examined histopathologically by light microscopy.

Echocardiography

Sixteen 10-wk-old Wistar rats (body weight, 308 ± 15.6 g) were anesthetized (sodium pentobarbital, 30 mg/kg intraperitoneally) for a baseline ventricular function measurement by echocardiography (Sonos 5500 equipped with a 15-MHz phased-array transducer; Philips Electronics N.V.). The anesthetized rats were subjected to 20 min of myocardial ischemia and 30 min of reperfusion. Half the animals received a single intravenous injection of EPO (200 units/kg in 0.3 mL of saline) immediately after LCA occlusion (EPO group). The other rats received an equivalent volume of saline at the same time point (nT group). Echocardiography was performed immediately after release of the LCA occlusion and repeated at 2 and 4 wk after surgery. A parasternal long-axis view was recorded, ensuring that the mitral and aortic valves and the apex were visualized. A short-axis view was recorded at the level of the mid papillary muscles. Both 2-dimensional and motion-mode views were recorded at the same level. LV end-diastolic dimension (Dd) and end-systolic dimension (Ds) were measured from motion mode in both short- and long-axis views. The LV percentage of fractional shortening (%FS) in the long-axis view was calculated as %FS = (Dd − Ds)/Dd × 100. All measurements were taken and averaged over 5 consecutive cardiac cycles by 1 observer who was unaware of the treatment with EPO. The reproducibility of measurements was assessed at baseline by 2 sets of measurements in 10 randomly selected rats. The repeated-measures variability did not exceed ±5%. Blood (0.5 mL) was collected from the jugular vein under pentobarbital anesthesia just before and after operation and at 4, 10, and 28 d after operation to determine the hematocrit level (measured in triplicate).

Statistical Analysis

Results were expressed as mean ± SD. Statistical analyses were performed using a Windows computer with StatView software (version 5.0; SAS Institute Inc.). Comparisons between the 2 groups were made using an unpaired *t* test. The time course of the changes was compared by repeated-measures ANOVA with the Scheffé post hoc test. The relationship of ^{99m}Tc-annexin V uptake in the area at risk was correlated with the number of TUNEL-positive cells by linear regression. A value of P less than 0.05 was considered statistically significant.

RESULTS

Autoradiographic Detection of Early Apoptotic Cells

Representative images of dual autoradiography are shown in Figure 1. In the nT group, ^{99m}Tc-annexin V accumulated strongly at the central zone of the myocardial area at risk, predominantly in the mid layer of myocardium. Compared with the nT group, the accumulation of ^{99m}Tc-annexin V was reduced in the EPO group. The areas of ^{99m}Tc-annexin V accumulation were smaller in the EPO group than in the nT group. Quantitative analyses demonstrated that the area ratio and density ratio of the EPO group were significantly smaller than those of the nT group (area ratio, 0.318 ± 0.038 vs. 0.843 ± 0.051, $P < 0.001$; density ratio, 22.2 ± 4.2 vs. 108.3 ± 14.0, $P < 0.0001$) (Fig. 2). The ^{201}Tl transmural defect areas of these 2 groups did not significantly differ in size (24.8 ± 2.1 vs. 25.9 ± 2.6 mm^2, $P = 0.56$).

Comparison of Histologic Findings with ^{99m}Tc-Annexin V Autoradiography

Figure 3 showed the representative tissue sections of TUNEL staining in each group. The myocardium in both groups showed no inflammatory cells, no necrotic cells, and no myocardial degeneration on the light microscopic examination of the hematoxylin- and eosin-stained slices. TUNEL-positive cells were scattered at the mid layer of the myocardial area at risk in the nT group. In contrast, TUNEL-positive cells were localized to a small area in the EPO group. In both groups, the distribution of TUNEL-positive cells agreed closely with

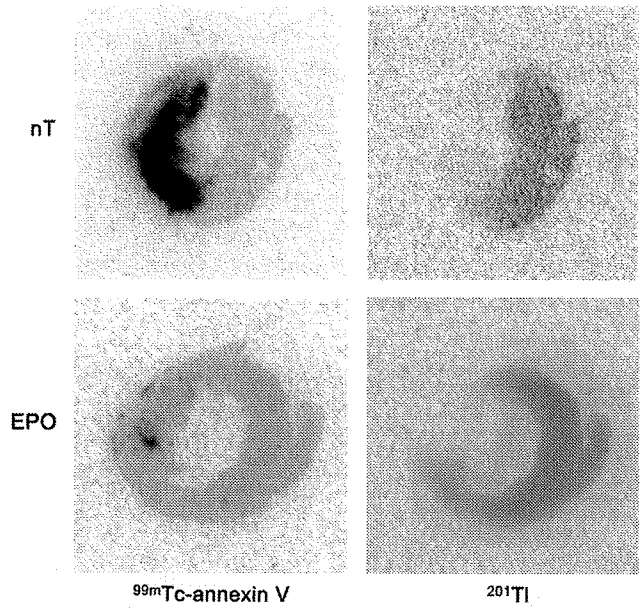

FIGURE 1. Autoradiography of ^{99m}Tc-annexin V and ^{201}Tl. Midventricular slices are shown from representative animals from each group. ^{99m}Tc-annexin V uptake area indicates myocardial apoptotic area, whereas ^{201}Tl defect area demonstrates area at risk. In nT group, ^{99m}Tc-annexin V highly accumulated at central zone of myocardial area at risk. Compared with nT group, accumulation of ^{99m}Tc-annexin V was reduced in EPO group with regard to both size and density.

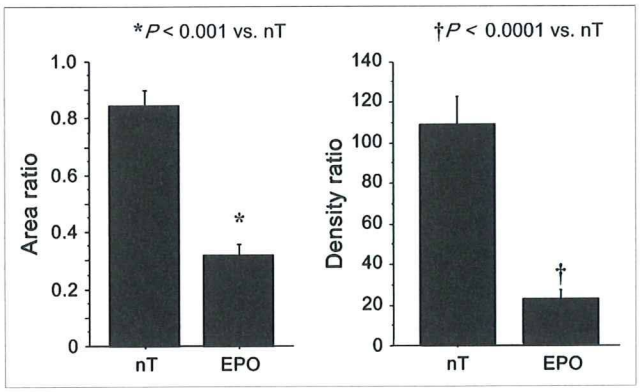

FIGURE 2. Area ratio calculated by dividing ^{99m}Tc-annexin V uptake area by ^{201}Tl defect area would indicate extent of apoptotic area in area at risk. Density ratio calculated by dividing uptake value of ^{99m}Tc-annexin V uptake area by that of normally perfused area would reflect intensity of apoptosis in apoptotic area. Area ratio and density ratio of EPO group were significantly smaller than those of nT group (area ratio: 0.318 ± 0.038 vs. 0.843 ± 0.051, $P < 0.001$; density ratio: 22.2 ± 4.2 vs 108.3 ± 14.0, $P < 0.0001$).

^{99m}Tc-annexin V accumulation. Moreover, the density of the TUNEL-positive cells (the number of TUNEL-positive cells per high-power field [HPF]) in the EPO group was significantly smaller than that in the nT group (34.1 ± 11.7/HPF vs. 136.8 ± 25.9/HPF, $P < 0.01$) (Fig. 4).

Figure 5 compares the density of TUNEL-positive cells in the representative myocardial apoptotic area (the number of TUNEL-positive cells per HPF) of each rat with the density of ^{99m}Tc-annexin V accumulation (PSL/m^2) in the corresponding area. The density of ^{99m}Tc-annexin V accumulation correlated well with the density of TUNEL-positive cells ($r = 0.886$, $P < 0.01$).

The Influence of EPO on Hematocrit

The average changes in hematocrit in rats treated with EPO (200 units/kg in 0.3 mL of saline) did not differ from those receiving an equivalent volume of saline just before and after operation and at 4, 10, and 28 d after operation (Table 1).

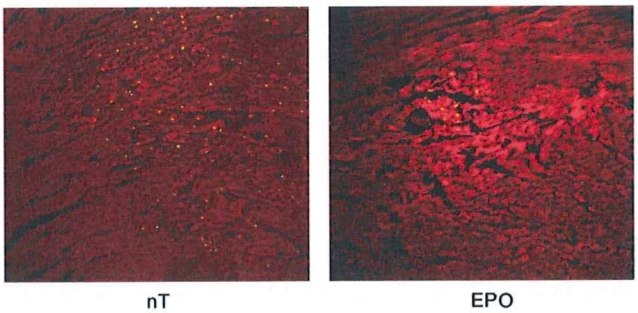

FIGURE 3. Representative tissue section of TUNEL staining is shown in each group. TUNEL-positive cells were scattered at mid layer of myocardial area at risk in nT group. In contrast, TUNEL-positive cells were localized to very small area in EPO group.

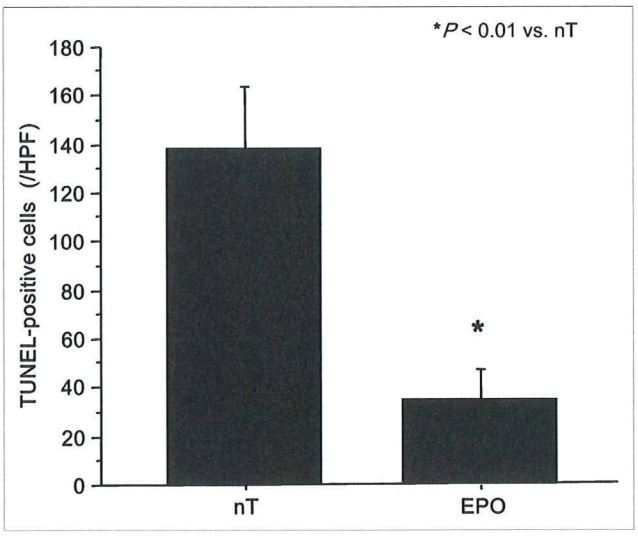

FIGURE 4. Tissue sections of TUNEL staining were observed under confocal microscopy at 200× magnification. Density of TUNEL-positive cells (number of TUNEL-positive cells per HPF) in EPO group was significantly smaller than that of nT group (34.1 ± 11.7/HPF vs. 136.8 ± 25.9/HPF, $P < 0.01$).

Echocardiography

Baseline (presurgery) measurements of LV cavity size (Dd) and LV systolic function (%FS) were similar in the groups assigned to EPO and nT. After coronary ligation/release, the depression in ejection fraction (36.1 ± 3.9 vs. 36.8 ± 3.1, $P = 0.91$) was similar in the 2 groups (Table 2).

Figure 6 illustrates the average changes in Dd and %FS at 2 and 4 wk after ischemia–reperfusion injury. In the nT group, Dd increased to a greater extent from 0 to 2 wk than from 2 to 4 wk. The percentage change in Dd at 2 and 4 wk after the surgical procedure, compared with baseline data immediately after ischemia–reperfusion injury, was 34.7% ±

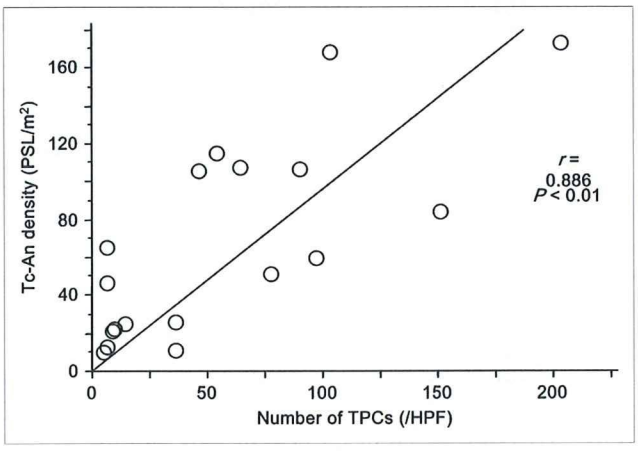

FIGURE 5. Comparison of density of TUNEL-positive cells in representative myocardial apoptotic area (number of TUNEL-positive cells per HPF) of each rat with density of ^{99m}Tc-annexin V accumulation (PSL/m^2) in corresponding area. Density of ^{99m}Tc-annexin V accumulation correlated well with density of TUNEL-positive cells ($r = 0.886$, $P < 0.01$).

TABLE 1
Serial Measurements of Hematocrit After a Single Administration of EPO or Saline

Administered substance	Just before operation	Just after operation	Day 4	Day 10	Day 28
Saline (6)	40.9 ± 0.4	41.9 ± 0.4	42.6 ± 0.7	41.6 ± 0.4	40.9 ± 0.6
EPO (6)	40.1 ± 0.3	41.1 ± 0.4	42.3 ± 0.5	42.4 ± 0.5	42.6 ± 0.8

Data are mean percentage ± SD.

3.8% and 34.9% ± 5.0%, respectively. On the other hand, in the EPO group, the percentage change in Dd at 2 and 4 wk after ischemia–reperfusion injury was just 8.5% ± 2.1% ($P < 0.01$ vs. nT at 2 wk) and 13.2% ± 2.8% ($P < 0.01$ vs. nT at 4 wk), respectively.

A significant difference was observed in %FS between the EPO and nT groups over the 4-wk follow-up. Compared with the baseline data immediately after ischemia–reperfusion injury, %FS in the nT group declined by 42.2% ± 3.4% and 52.9% ± 3.4% at 2 and 4 wk. The LV performance of the nT group declined more steeply from 0 to 2 wk than from 2 to 4 wk. The %FS in the EPO group decreased slightly at 2 wk (−9.0% ± 1.9%, $P < 0.01$, vs. nT at 2 wk) and 4 wk (−11.1% ± 6.7%, $P < 0.01$, vs. nT at 4 wk).

These data suggest that the marked enlargement of the LV cavity and the steep decline of LV contractile function occurring in the nT group in the 2 wk after occlusion/release was suppressed by a single injection of EPO.

DISCUSSION

In this study, the extent of apoptosis after ischemia–reperfusion injury was markedly reduced after a single intravenous dose of EPO. This reduction of apoptosis was seen in histologic TUNEL staining of the myocardium in the area at risk and in autoradiographic studies with ^{99m}Tc-annexin V within 1 h of EPO administration. Moreover, echocardiography demonstrated that a single systemic administration of EPO immediately after coronary ligation minimized LV remodeling and preserved contractile function at 2 and 4 wk after surgery.

^{99m}Tc-annexin V has been reported to be highly sensitive in detecting apoptosis immediately after ischemia–reperfusion myocardial injury (*24,25*). ^{99m}Tc-annexin V has been used to image injured myocardium after acute MI in patients undergoing acute coronary angioplasty (*26*). In 6 of 7 patients, increased uptake of ^{99m}Tc-annexin V was seen in the infarct area of the heart on early and late SPECT images, suggesting that apoptosis occurs in that area. Taki et al. reported similar findings with ^{99m}Tc-annexin V localization in the area at risk early after ischemia–reperfusion injury (*14*). The concentration of ^{99m}Tc-annexin V in the area at risk was concordant with the distribution of TUNEL-positive cells. In their study, ^{99m}Tc-annexin V accumulation was most prominent at 30–90 min after reperfusion and then gradually declined, whereas the number of TUNEL-positive cells peaked at 6 h to 1 d after reperfusion. In our study, ^{99m}Tc-annexin V accumulation clearly delineated the area of the apoptotic myocardium in the 20-min occlusion/30-min reperfusion model, consistent with the results of previous studies (*14,24,25,*). The previous investigation reported that, with TUNEL staining, EPO can limit the size of LV infarction (*12*). In this study, EPO therapy caused a 2.7-fold reduction of ^{99m}Tc-annexin V accumulation in the ischemic risk area.

Previous studies reported that a single administration of EPO increased the number of circulating reticulocytes by 3–4 d (reaching a maximum by days 8–11) (*27,28*). In the present study, the hematocrit in the rats treated with EPO did not differ from that in rats receiving saline just after operation and at 4, 10, and 28 d after operation. Therefore, the response

TABLE 2
Baseline Echocardiographic Parameters in EPO-Treated and Control Rats

Index	Group	Before operation	After operation
LVDd (mm)	nT	6.2 ± 0.1	6.5 ± 0.2
	EPO	6.3 ± 0.1	6.6 ± 0.2
%FS	nT	61.3 ± 1.3	36.8 ± 3.1
	EPO	62.2 ± 0.9	36.1 ± 3.9

Data are mean ± SD.

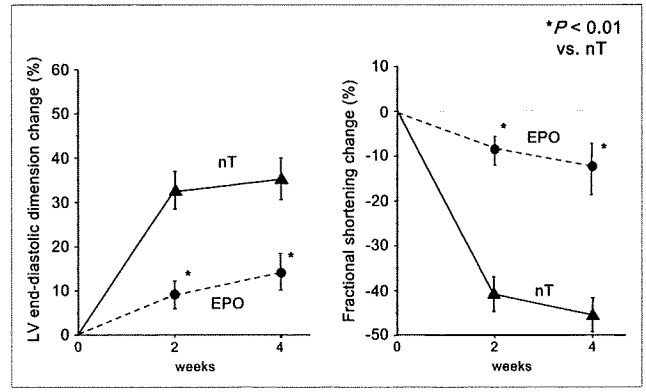

FIGURE 6. Changes in echocardiographic indices of LV size (Dd) and function (fractional shortening) during 4 wk after ischemia–reperfusion injury in EPO-treated and untreated rats. All indices are expressed as percentage change from baseline values (Table 2). *Significant difference ($P < 0.01$) between nT and EPO groups in percentage change in LV Dd and fractional shortening at weeks 2 and 4.

seen in the current experiment is unlikely related to an increase in the oxygen-carrying capacity of the blood.

The cardio- and neuroprotective properties are likely due to the interaction of EPO with the common β-receptor. This receptor requires a higher concentration of EPO and has the effect of reducing apoptosis. Previous studies in a rabbit model demonstrated that a single dose of EPO (5,000 units/kg) reduced infarct size from 35% to 13.8%, in keeping with the results in the present study (*3*). This acute effect persists over the subsequent 4-wk interval of observation. Previous observations have demonstrated a favorable influence of the antiapoptotic effect of EPO on long-term LV chamber size and function after myocardial ischemia (*12,13*). Moon et al. showed that a single dose of EPO at the onset of myocardial infarction reduced infarct size and reduced LV remodeling and dysfunction measured by echocardiography during the subsequent 8-wk period (*12*). Our results confirm that a single intravenous injection of EPO immediately after coronary occlusion suppressed LV remodeling and contractile deterioration at 4 wk after surgery. The results of ^{99m}Tc-annexin V autoradiography and TUNEL staining suggest that the beneficial effect of EPO is due to a remarkable suppression of apoptosis in the area at risk in this rat ischemia–reperfusion injury model. The mechanism of apoptosis reduction may be due to a phosphatidylinositol-3 kinase/Akt dependent pathway, as demonstrated in vivo in dog hearts (*29*).

Although prolonged administration of EPO is associated with adverse effects related to hematocrit elevation, such as hypertension and thromboembolic complications (*30,31*), a single administration of EPO, even at the higher doses used in this study, had a beneficial effect on the preservation of cardiac function after ischemia–reperfusion injury.

This study had 2 limitations. The first was the inability to assess the other effects of EPO on LV remodeling and function after myocardial infarction, though more recent studies reported that EPO possesses proangiogenic properties promoting neovascularization related to infarct size reduction after myocardial infarction (*32*). The second limitation was that we studied the feasibility of ^{99m}Tc-annexin V to assess the antiapoptotic treatment of EPO at only 1 time point, 30 min after the beginning of reperfusion. Further examination is needed to know the optimal timing for EPO injection as well as the optimum time for ^{99m}Tc-annexin V injection and imaging to assess the cardioprotective effect of EPO.

CONCLUSION

The present study demonstrated that ^{99m}Tc-annexin V is useful to evaluate myocardial apoptosis associated with ischemia–reperfusion injury. The ratio of the perfusion area at risk to annexin V lesion size is a useful indicator of myocardium salvaged by acute administration of EPO. The echocardiographic study showed that a single treatment with EPO immediately after coronary ligation suppressed cardiac remodeling and functional deterioration for at least 4 wk after the acute insult. These studies suggest that a single dose of EPO may be useful to prevent long-term cardiac remodeling and dysfunction after ischemia–reperfusion injury.

ACKNOWLEDGMENT

We thank Nihon Medi-Physics Co., Ltd., for its constant support, inclusive of radioisotope supply. This study was supported in part by grant-in-aid B-18790919 for young scientists from the Ministry of Education, Science, Sports, and Culture, Japan.

REFERENCES

1. Fliss H, Gautinger D. Apoptosis in ischemic and reperfused rat myocardium. *Circ Res.* 1996;79:949–956.
2. Gottlieb RA, Burleson KO, Kloner RA, et al. Reperfusion injury induces apoptosis in rabbit cardiomyocytes. *J Clin Invest.* 1994;94:1621–1628.
3. Parsa CJ, Matsumoto A, Kim J, et al. A novel protective effect of erythropoietin in the infarcted heart. *J Clin Invest.* 2003;112:999–1007.
4. Cai Z, Semenza GL. Phosphatidylinositol-3-kinase signaling is required for erythropoietin-mediated acute protection against myocardial ischemia/reperfusion injury. *Circulation.* 2004;109:2050–2053.
5. Maulik N, Kagan VE, Tyurin VA, et al. Redistribution of phosphatidylethanolamine and phosphatidylserine precedes reperfusion-induced apoptosis. *Am J Physiol.* 1998;274:H242–H248.
6. Martin SJ, Reutelingsperger CP, McGahon AJ, et al. Early redistribution of plasma membrane phosphatidylserine is a general feature of apoptosis regardless of the initiating stimulus: inhibition by overexpression of Bcl-2 and Abl. *J Exp Med.* 1995;182:1545–1556.
7. Digicaylioglu M, Bichet S, Marti HH, et al. Localization of specific erythropoietin binding sites in defined areas of the mouse brain. *Proc Natl Acad Sci USA.* 1995;92:3717–3720.
8. Ehrenreich H, Hasselblatt M, Dembowski C, et al. Erythropoietin therapy for acute stroke is both safe and beneficial. *Mol Med.* 2002;8:495–505.
9. Sakanaka M, Wen TC, Matsuda S, et al. In vivo evidence that erythropoietin protects neurons from ischemic damage. *Proc Natl Acad Sci USA.* 1998;95:4635–4640.
10. Brines M, Grasso G, Fiordaliso F, et al. Erythropoietin mediates tissue protection through an erythropoietin and common beta-subunit heteroreceptor. *Proc Natl Acad Sci USA.* 2004;101:14907–14912.
11. Calvillo L, Latini R, Kajstura J, et al. Recombinant human erythropoietin protects the myocardium from ischemia-reperfusion injury and promotes beneficial remodeling. *Proc Natl Acad Sci USA.* 2003;100:4802–4806.
12. Moon C, Krawczyk M, Ahn D, et al. Erythropoietin reduces myocardial infarction and left ventricular functional decline after coronary artery ligation in rats. *Proc Natl Acad Sci USA.* 2003;100:11612–11617.
13. Parsa CJ, Jihee K, Riel RU, et al. Cardioprotective effect of erythropoietin in the reperfused ischemic heart. *J Biol Chem.* 2004;279:20655–20662.
14. Taki J, Higuchi T, Kawashima A, et al. Detection of cardiomyocyte death in a rat model of ischemia and reperfusion using ^{99m}Tc-annexin V. *J Nucl Med.* 2004;45:1536–1541.
15. Zwaal RFA, Schroit AJ. Pathophysiologic implications of membrane phospholipids asymmetry in blood cells. *Blood.* 1997;89:1121–1132.
16. Blankenberg FG, Katsikis PD, Tait JF, et al. In vivo detection and imaging of phosphatidylserine expression during programmed cell death. *Proc Natl Acad Sci USA.* 1998;95:6349–6354.
17. Blankenberg FG, Katsikis PD, Tait JF, et al. Imaging of apoptosis (programmed cell death) with ^{99m}Tc-labeled annexin V. *J Nucl Med.* 1999;40:184–191.
18. Fadok VA, Laszlo DJ, Noble PW, Weinstein L, Riches DW, Henson PM. Particle digestibility is required for induction of the phosphatidylserine recognition mechanism used by murine macrophages to phagocytose apoptotic cells. *J Immunol.* 1993;151:4274–4285.
19. Koopman G, Reutelingsperger CP, Kuijten GA, Keehnen RM, Pals ST, van Oers MH. Annexin V for flow cytometric detection of phosphatidylserine expression on B cells undergoing apoptosis. *Blood.* 1994;84:1415–1420.
20. Narula J, Acio ER, Narula N, et al. Annexin-V imaging for noninvasive detection of cardiac allograft rejection. *Nat Med.* 2001;7:1347–1352.
21. Peker C, Sarda-Mantel L, Loiseau P, et al. Imaging apoptosis with ^{99m}Tc-labeled annexin V in experimental subacute myocarditis. *J Nucl Med.* 2004;45:1081–1086.

22. Bennink RJ, van den Hoff MJ, van Hemert FJ, et al. Annexin V imaging of acute doxorubicin cardiotoxicity (apoptosis) in rats. *J Nucl Med.* 2004;45:842–848.
23. Tait JF, Brown DS, Gibson DF, et al. Development and characterization of annexin V mutants with endogenous chelation sites for ^{99m}Tc. *Bioconjug Chem.* 2000;11:918–925.
24. Dumont EA, Reutelingsperger CP, Smits JF, et al. Real-time imaging of apoptotic cell-membrane changes at the single-cell level in the beating murine heart. *Nat Med.* 2001;7:1352–1355.
25. Dumont EA, Hofstra L, van Heerde WL, et al. Cardiomyocyte death induced by myocardial ischemia and reperfusion: measurement with recombinant human annexin-V in a mouse model. *Circulation.* 2000;102:1564–1568.
26. Hofstra L, Liem IH, Dumont EA, et al. Visualisation of cell death in vivo in patients with acute myocardial infarction. *Lancet.* 2000;356:209–212.
27. Cheung WK, Goon BL, Guilfoile MC, et al. Pharmacokinetics and pharmacodynamics of recombinant human erythropoietin after single and multiple subcutaneous doses to healthy subjects. *Clin Pharmacol Ther.* 1998;64:412–423.
28. Eder H, Rosslenbroich B, Failing K. Erythropoietin reduces myocardial infarction and left ventricular functional decline after coronary artery ligation in rats. *Blut.* 1989;59:184–187.
29. Hirata A, Minamino T, Asanuma H, et al. Erythropoietin just before reperfusion reduces both lethal arrhythmias and infarct size via the phosphatidylinositol-3 kinase-dependent pathway in canine hearts. *Cardiovasc Drugs Ther.* 2005;19: 33–40.
30. Roger SD, Baker LR, Raine AE. Autonomic dysfunction and the development of hypertension in patients treated with recombinant human erythropoietin (r-HuEPO). *Clin Nephrol.* 1993;39:103–110.
31. Wolf RF, Gilmore LS, Friese P, Downs T, Burstein SA, Dale GL. Erythropoietin potentiates thrombus development in a canine arteriovenous shunt model. *Thromb Haemost.* 1997;77:1020–1024.
32. van der Meer P, Lipsic E, Henning RH, et al. Erythropoietin induces neovascularization and improves cardiac function in rats with heart failure after myocardial infarction. *J Am Coll Cardiol.* 2005;46:125–133.

Available online at www.sciencedirect.com
ScienceDirect
Nuclear Medicine and Biology 35 (2008) 213–218
NUCLEAR MEDICINE — AND — BIOLOGY
www.elsevier.com/locate/nucmedbio

Evaluation of radioiodinated (2*S*,α*S*)-2-(α-(2-iodophenoxy)benzyl) morpholine as a radioligand for imaging of norepinephrine transporter in the heart

Yasushi Kiyono[a,c,*], Taku Sugita[b], Masashi Ueda[c], Hidekazu Kawashima[d], Naoki Kanegawa[b], Yuji Kuge[b], Yasuhisa Fujibayashi[a], Hideo Saji[b]

[a]*Biomedical Imaging Research Center, University of Fukui, Fukui 910-1193, Japan*
[b]*Department of Pathofunctional Bioanalysis, Graduate School of Pharmaceutical Sciences, Kyoto University, Kyoto 606-8501, Japan*
[c]*Radioisotopes Research Laboratory, Kyoto University Hospital, Faculty of Medicine, Kyoto University, Kyoto 606-8507, Japan*
[d]*Department of Nuclear Medicine and Diagnostic Imaging, Graduate School of Medicine, Kyoto University, Kyoto 606-8507, Japan*

Received 5 September 2007; received in revised form 23 November 2007; accepted 23 November 2007

Abstract

Introduction: The norepinephrine transporter (NET) is located presynaptically on noradrenergic nerve terminals and plays a critical role in the regulation of the synaptic norepinephrine (NE) concentration via the reuptake of NE. Changes in NET have been recently reported in several cardiac failures. Therefore, a NET-specific radioligand is useful for in vivo assessment of changes in NET density in various cardiac disorders. Recently, we developed a radioiodinated reboxetine analogue, (2*S*,α*S*)-2-(α-(2-iodophenoxy)benzyl)morpholine ((*S*,*S*)-IPBM), for NET imaging. In the current study, we assessed the applicability of radioiodinated (*S*,*S*)-IPBM to NET imaging in the heart.
Methods: The NET affinity and selectivity were measured from the ability to displace specific [^{3}H]nisoxetine and (*S*,*S*)-[^{125}I]IPBM binding to rat heart membrane, respectively. To evaluate the distribution of (*S*,*S*)-[^{125}I]IPBM in vivo, biodistribution experiment was performed in rats. With the use of several monoamine transporter binding agents, pharmacological blocking experiments were performed in rats.
Results: In vitro binding assays showed that the affinity of (*S*,*S*)-IPBM to NET was similar to those of the well-known NET-specific binding agents, nisoxetine and desipramine. Furthermore, (*S*,*S*)-[^{125}I]IPBM binding was inhibited by nisoxetine and desipramine, but not by dopamine or serotonin transporter binding agents. These data indicated that (*S*,*S*)-IPBM had high affinity and selectivity for NET in vitro. Biodistribution studies in rats showed rapid and high uptake of (*S*,*S*)-[^{125}I]IPBM by the heart and rapid clearance from the blood. The heart-to-blood ratio was 31.9 at 180 min after the injection. The administration of nisoxetine and desipramine decreased (*S*,*S*)-[^{125}I]IPBM accumulation in the heart, but injection of fluoxetine and GBR12909 had little influence.
Conclusions: Radioiodinated (*S*,*S*)-IPBM is a potential radioligand for NET imaging in the heart.

Keywords: Norepinephrine transporter; Sympathetic nervous function; SPECT; Radioiodination; (*S*,*S*)-IPBM; Heart

1. Introduction

The norepinephrine transporter (NET) is located presynaptically on noradrenergic nerve terminals and plays a critical role in the regulation of synaptic concentrations of norepinephrine (NE) in the noradrenergic nervous system by the reuptake of NE [1]. In the heart, NET exists in sympathetic nerve terminals. Changes in NET have been reported in several cardiac failures [2–7]. Furthermore, this NET has been recently noted as a therapeutic target [8–10]. Two pieces of information are necessary for estimating this NET function precisely. One is the transport activity of NET, and the other is the density of NET in sympathetic nerve terminals. To evaluate the first information, [^{123}I]meta-iodobenzylguanidine (MIBG) and [^{11}C]hydroxyephedrine, NET substrates, have been widely used for the imaging of cardiac

* Corresponding author. Biomedical Imaging Research Center, University of Fukui, 23-3, Matsuokashimoaizuki, Eiheiji, Yoshida, Fukui 910-1193, Japan. Tel.: +81 776 61 8420; fax: +81 776 61 8170.
E-mail address: ykiyono@u-fukui.ac.jp (Y. Kiyono).

0969-8051/$ – see front matter © 2008 Elsevier Inc. All rights reserved.
doi:10.1016/j.nucmedbio.2007.11.006

sympathetic nervous function in various cardiovascular diseases [11–13]. These radiolabeled NET substrates are taken up by sympathetic nerve terminals, stored into vesicles and secreted to sympathetic clefts, and therefore images of these NET substrates reflect the overall function of nervous terminals. The information on NET density could be also important for predicting the effect of NET targeting therapy and/or understanding the condition of cardiac diseases.

A radioligand bound to NET could be potentially useful for studying the role of the NE reuptake system in these diseased states and for predicting the therapeutic effect of NET targeting drugs. Therefore, the development of a radioligand to bind NET has been of great interest.

We recently synthesized radioiodinated (*R*)-*N*-methyl-3-(2-iodophenoxy)-3-phenylpropamine ((*R*)-MIPP) as a NET binding agent. However, this radioligand had a slight affinity to serotonin transporter (SERT) in vivo in the brain and heart [14,15]. More recently, we developed radioiodinated (2*S*,α*S*)-2-(α-(2-iodophenoxy)benzyl)morpholine ((*S*,*S*)-IPBM), which was more selective for NET compared with (*R*)-MIPP in the brain [15,16].

In this study, the applicability of radioiodinated (*S*,*S*)-IPBM to NET imaging in the heart was evaluated by investigating the affinity and selectivity for NET in the heart and biodistribution including pharmacological blocking experiments and comparison with MIBG.

2. Materials and methods

2.1. Materials

[^{125}I]MIBG was supplied by Daiichi Radioisotope Laboratories (Tokyo, Japan). Sodium [^{125}I]iodide (643.8 GBq/mg) and [^{3}H]nisoxetine (2.96 TBq/mmol) were purchased from New England Nuclear (Boston, MA, USA). All chemicals used in this study were of reagent grade.

2.2. Radiosynthesis

(*S*,*S*)-[^{125}I]IPBM was obtained by a halogen exchange reaction with sodium [^{125}I]iodine according to the methods of Kanegawa et al. [15]. Briefly, (*S*,*S*)-BPBM was added to a mixture of sodium [^{125}I]-iodine, ammonium sulfate and copper (II) sulfate pentahydrate in a vial. The reaction mixture was heated for 45 min at 130°C. After cooling, the reaction mixture was extracted with methanol and filtered with a 0.22-μm filter. The filtered extract was applied to a reverse-phase high-performance liquid chromatography (HPLC) column (Cosmosil 5C_{18}-AR-300 Packed Column, 250×10 mm id, Nacalai Tesque, Kyoto, Japan) and eluted with 20 mM phosphate buffer (pH 2.5)/acetonitrile=72:28 at a flow rate of 2.0 ml/min [R_t=42 min for (*S*,*S*)-BPBM, 58 min for (*S*,*S*)-IPBM]. An adequate amount of ethanol was added to the separated (*S*,*S*)-[^{125}I]-IPBM fraction.

The radiochemical purity of the labeled compound was determined by analytical HPLC. Analytical HPLC was performed on a 150×4.6 mm id, Cosmosil AR-300 column (Nacalai Tesque, Kyoto, Japan) eluted with 20 mM phosphate buffer (pH 2.5)/acetonitrile=72:28 at a flow rate of 1.0 ml/min (R_t=15.0 min).

2.3. In vitro binding assay

The preparation of synaptosomal membranes from rat hearts was carried out according to a previously reported method with some modifications [17]. Briefly, the heart ventricles were homogenized in 20 volumes of ice-cold 250 mM sucrose buffer (5 mM Tris/HCl; 1 mM $MgCl_2$; 250 mM sucrose) with a 30-s burst, using a Polytron PT10-35 set at speed 6. The homogenate was centrifuged at 750×*g* for 10 min. The pellet was discarded and the supernatant recentrifuged at 20,000×*g* for 20 min. The resulting pellet was resuspended in 10 volumes of ice-cold 50 mM Tris-HCl buffer (50 mM Tris/HCl, 5 mM KCl, 120 mM NaCl, pH 7.4) and recentrifuged to give a pellet that was resuspended in 5 vol of the Tris-HCl buffer. The suspension was stored at −80°C until use. The protein concentration was measured by the Lowry method [18].

[^{3}H]Nisoxetine and (*S*,*S*)-[^{125}I]IPBM competition assays were performed according to the methods of Raisman et al. [17] with some modification. The assays were carried out by incubating 400 μl of the heart preparation (0.25 mg/ml) with [^{3}H]nisoxetine (2.5 nM) and various concentrations of competitors in 150 μl of 50 mM Tris-HCl buffer (50 mM Tris/HCl, 5 mM KCl, 120 mM NaCl, pH 7.4). Incubation was performed for 30 min at 25°C. At the end of the incubation, the mixture was poured into 5 ml of ice-cold Tris-HCl buffer, rapidly filtered through Whatman GF/B fiber filters and washed with 3×5 ml of buffer. For [^{3}H] nisoxetine, the radioactivity bound to the filter was measured with a liquid scintillation counter (2500-TR, Packard). For (*S*,*S*)-[^{125}I]IPBM, the radioactivity bound to the filters was measured with a NaI well scintilation counter (Cobra II Auto-Gamma, Packard). All incubations were performed in triplicate. Nonspecific binding was determined in the presence of 1 mM nisoxetine. IC_{50} values were determined from displacement curves of the percent inhibition of [^{3}H] nisoxetine and (*S*,*S*)-[^{125}I]IPBM binding vs. the inhibitor concentration using the GraphPad Prism software (GraphPad Software, San Diego, CA, USA).

(*S*,*S*)-[^{125}I]IPBM saturation assays were performed according to our previous method for brain with some modification [16]. Four hundred microliters of membrane (0.25 mg/ml) was mixed with 50 μl of (*S*,*S*)-[^{125}I]IPBM (0.01–3.0 nM). Incubation was performed for 60 min at 25°C. At the end of the incubation, the mixture was poured into 5 ml of ice-cold Tris-HCl buffer, rapidly filtered through Whatman GF/B fiber filters and washed with 3×5 ml of buffer, and the radioactivity was measured with a NaI well scintilation counter. Nonspecific binding was determined in the presence of 1 mM nisoxetine. K_D value was determined with GraphPad Prism.

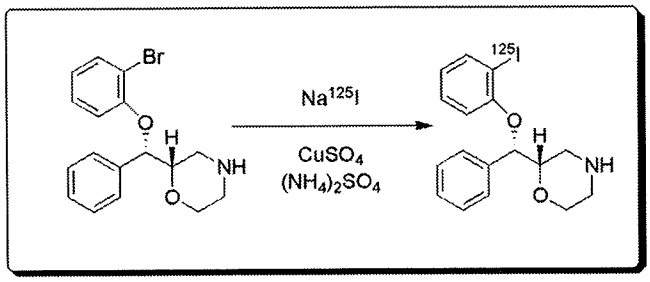

Fig. 1. Radiosynthesis of (*S,S*)-[^{125}I]IPBM.

2.4. Animals

Animal studies were conducted in accordance with our institutional guidelines, and the experimental procedures were approved by the Kyoto University Animal Care Committee.

2.5. Biodistribution experiments

Biodistribution studies were performed by intravenous administration of (*S,S*)-[^{125}I]IPBM (74 kBq) to 10-week-old male Sprague-Dawley rats. At appropriate time points after the administration, rats were sacrificed by decapitation under light ether anesthesia. Samples of blood and the organ of interest were excised and weighed, and the radioactivity was measured with an auto-well gamma counter (Aloka ARC2000, Tokyo, Japan).

2.6. Pharmacological blocking experiments

For pharmacological blocking studies, Sprague-Dawley rats were intravenously injected with (*S,S*)-[^{125}I]IPBM and various inhibitors. Nisoxetine (1 mg/kg) and desipramine (1 mg/kg) were used as NET binding agents. Fluoxetine (1 mg/kg) was used as a SERT binding agent. GBR12909 (1 mg/kg) was used for the dopamine transporter (DAT) binding agent. These agents were simultaneously injected with (*S,S*)-[^{125}I] IPBM. The animals were sacrificed 60 min after receiving (*R*)-[^{125}I]IPBM.

2.7. MIBG biodistribution experiments

To assess the potential of cardiac sympathetic nervous imaging agent, the comparison with MIBG was performed. [^{125}I]MIBG (74 kBq) was intravenously injected to 10-week-old male Sprague-Dawley rats. At 15, 60 and 180 min postinjection, rats were sacrificed by decapitation under light ether anesthesia. Samples of blood and the organ of heart and liver were excised and weighed, and the radioactivity was measured with an auto-well gamma counter.

Table 1
Inhibition of [^{3}H]nisoxetine binding to rat heart membrane

Compound	IC_{50} (nM)
(*RR/SS*)-IPBM	22.0±7.22
(*SS*)-IPBM	10.9±6.82
(*RR*)-IPBM	67.6±13.7
Nisoxetine	9.00±0.84
Desipramine	5.96±0.83
Reboxetine	16.0±5.59

Each value represents the mean±S.D. of three independent experiments.

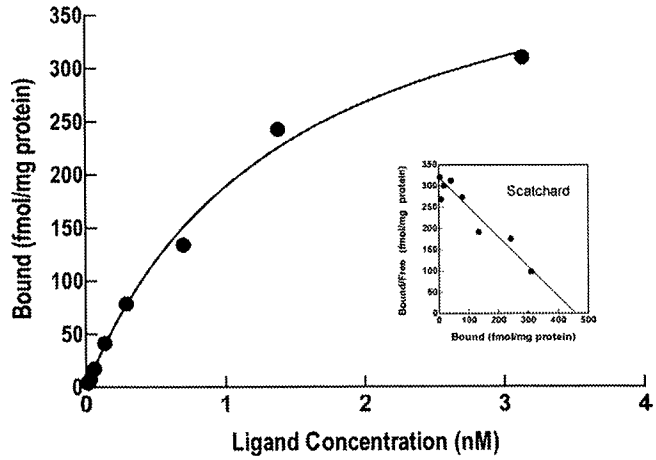

Fig. 2. Scatchard analysis of (*S,S*)-IPBM binding to rat heart membranes. The binding affinity was 1.63±0.22 nM.

2.8. Statistical analyses

Data are presented as mean values with the S.D. Comparisons were performed with the unpaired alternate Welch *t*-test. $P<.05$ was considered statistically significant.

3. Results

3.1. Radiosynthesis

The synthesis of no-carrier-added (*S,S*)-[^{125}I]IPBM was carried out by bromine-radioiodine exchange reaction (Fig. 1). The radiochemical yield of (*S,S*)-[^{125}I]IPBM was about 65% and the radiochemical purity was greater than 99%.

3.2. In vitro binding assay

In vitro binding assays showed that the affinity of (*S,S*)-IPBM (IC_{50}=10.9 nM) to NET was similar to those of the well-known NET inhibitors, nisoxetine and desipramine (IC_{50}=9.0 and 6.0 nM; Table 1). The specific binding of (*S,S*)-IPBM was saturable with a high affinity, and Scatchard transformation of the binding data gave a linear plot

Table 2
Inhibition of (*S,S*)-[^{125}I]IPBM binding to rat heart membrane

Compound	IC_{50} (nM)
Nisoxetine	2.28±0.87
Desipramine	6.86±2.71
Fluoxetine	1165±204
GBR12909	>10,000

Each value represents the mean±S.D. of three independent experiments.

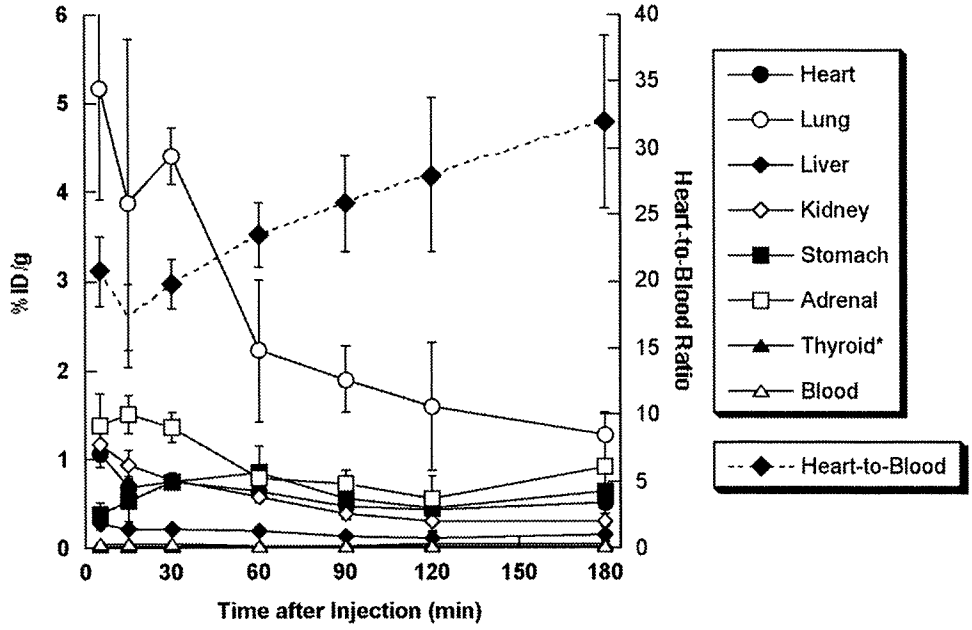

Fig. 3. Biodistribution of (*S,S*)-[^{125}I]IPBM in rats. Biodistribution of radioactivity is expressed as percentage of injected ^{125}I dose/gram of organ. Each point represents the mean±S.D. Only the data of thyroid represent the percentage of injected ^{125}I/organ.

indicating one-site binding (Fig. 2). The mean values gave a K_D value of 1.63±0.22 nM. Furthermore, (*S,S*)-[^{125}I]IPBM binding was inhibited by NET inhibitors, nisoxetine and desipramine (IC_{50}=2.28 and 6.86 nM; Table 2). However, (*S,S*)-[^{125}I]IPBM binding was only slightly inhibited by fluoxetine (IC_{50}=1165 nM; Table 2) and hardly inhibited at all by GBR12909 (IC_{50} >10,000 nM; Table 2). These data indicate that (*S,S*)-IPBM has a high affinity and selectivity for NET in vitro.

3.3. Biodistribution experiments

Fig. 3 shows the results of biodistribution studies in rats. The results showed rapid and high uptake of (*S,S*)-[^{125}I]IPBM by the heart and rapid clearance from the blood. The heart-to-blood ratio was increased with time, and the maximum value was 31.9 at 180 min after the injection. A high accumulation of (*S,S*)-[^{125}I]IPBM was observed in the lungs and adrenals, in which NET was abundant. The radioactivity in the liver was low. The level of radioactivity in the thyroid was also low, which indicated high stability of (*S,S*)-[^{125}I]IPBM to in vivo deiodination.

3.4. Pharmacological blocking experiments

The effects of various monoamine transporter inhibitors on the heart uptake of (*S,S*)-[^{125}I]IPBM were studied. Injection of nisoxetine and desipramine, NET binding agents, decreased the accumulation of (*S,S*)-[^{125}I]IPBM in the heart to about 40% at 60 min after injection (Fig. 4). However, the administration of fluoxetine and GBR12909 did not have significant effects on the accumulation of (*S,S*)-[^{125}I]IPBM in the heart.

3.5. Comparison of the biodistribution of (S,S)-[^{125}I]IPBM with [^{125}I]MIBG

The comparison of the biodistribution of (*S,S*)-[^{125}I]IPBM with [^{125}I]MIBG in 15-, 60- and 180-min phases is summarized in Table 3. The heart uptake of [^{125}I]MIBG was higher than that of (*S,S*)-[^{125}I]IPBM in each time point.

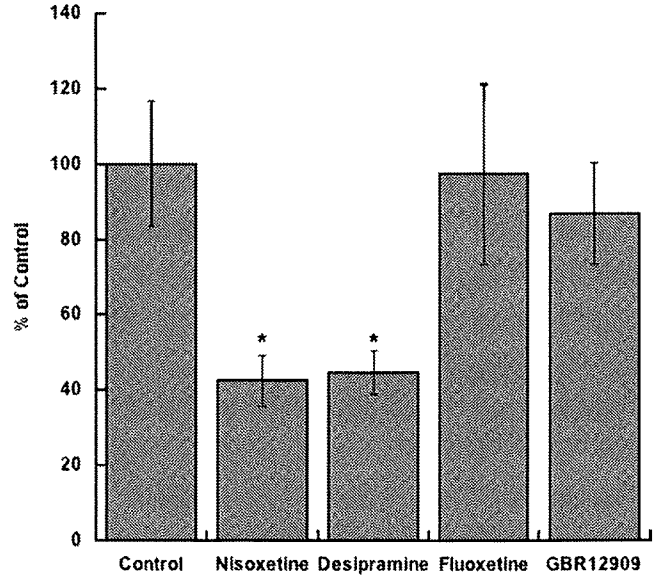

Fig. 4. Effect of various inhibitors on the cardiac uptake of (*S,S*)-[^{125}I]IPBM in rats. (*S,S*)-[^{125}I]IPBM was simultaneously injected with NET inhibitors, nisoxetine (1 mg/kg) and desipramine (1 mg/kg); a SERT inhibitor, fluoxetine (1 mg/kg); and a DAT inhibitor, GBR12909 (1 mg/kg). Rats were sacrificed at 60 min after injection. *P<.001 vs. control.

Table 3
Biodistributiion of (*S*,*S*)-[^{125}I]IPBM compared with [^{125}I]MIBG

		15 min	60 min	180 min
Heart	IPBM	0.66±0.13	0.64±0.07	0.50±0.13
	MIBG	2.78±0.22	1.95±0.85	2.11±0.17
Liver	IPBM	0.20±0.03	0.20±0.02	0.15±0.03
	MIBG	0.75±0.14	0.29±0.11	0.18±0.03
Blood	IPBM	0.039±0.007	0.027±0.003	0.016±0.003
	MIBG	0.18±0.04	0.13±0.06	0.12±0.02
Heart/blood ratio	IPBM	17.3±2.45	23.5±2.38	31.9±6.44
	MIBG	16.4±3.78	15.7±5.79	18.3±1.51

Biodistribution of radioactivity is expressed as percentage of injected ^{125}I dose/gram of organ (mean±S.D.).

Regarding liver uptake, the uptake of [^{125}I]MIBG in 15 and 60 min was higher than that of (*S*,*S*)-[^{125}I]IPBM. However, there was no significant difference in 180 min. The heart-to-blood ratio of (*S*,*S*)-[^{125}I]IPBM was higher than that of [^{125}I] MIBG in each time point.

4. Discussion

The basic requirements for an effective radiolabeled NET binding agent for molecular imaging of cardiac NET density include a high binding affinity and selectivity for the NET protein, and high heart uptake.

With respect to the affinity and selectivity, in vitro binding studies using the heart synaptosomal membranes showed that (*S*,*S*)-IPBM had a high affinity as well as nisoxetine, desipramine and reboxetine, the typical NET binding agents (Table 1). Furthermore, nisoxetine and desipramine inhibited the (*S*,*S*)-[^{125}I]IPBM binding, but fluoxetine slightly inhibited that binding and GBR12909 did not (Table 2). These results show that (*S*,*S*)-[^{125}I]IPBM has high affinity and selectivity for myocardial NET.

In biodistribution studies, (*S*,*S*)-[^{125}I]IPBM showed a high uptake followed by a rapid clearance in the heart. This distribution pattern in the heart was consistent with that of other radioligands for NET imaging [14,19,20]. Compared with (*R*)-[^{125}I]MIPP, the initial uptake of (*S*,*S*)-[^{125}I]IPBM was slightly lower [(*S*,*S*)-IPBM: 1.06 %ID/g, (*R*)-MIPP: 1.36 %ID/g, at 5 min postinjection]. However, at 180 min postinjection, accumulation of (*S*,*S*)-IPBM was higher than that of (*R*)-MIPP [(*S*,*S*)-IPBM: 0.50 %ID/g, (*R*)-MIPP: 0.27 %ID/g] [14]. These data suggest that the clearance of (*S*,*S*)-IPBM was slower than that of (*R*)-MIPP because (*S*,*S*)-IPBM bound to NET more selectively than (*R*)-MIPP. Furthermore, the heart-to-blood ratio of (*S*,*S*)-[^{125}I]IPBM was higher than that of (*R*)-[^{125}I]MIPP [(*S*,*S*)-IPBM: 23.5 (60 min) and 31.9 (180 min), (*R*)-MIPP: 13.0 (60 min) and 7.5 (180 min)] [14]. This is due to the higher accumulation of (*S*,*S*)-IPBM in the heart and faster clearance of (*S*,*S*)-IPBM from the blood. The administration of nisoxetine and desipramine, NET-specific binding agents, decreased (*S*,*S*)-[^{125}I]IPBM accumulation in the heart, but injection of fluoxetine and GBR12909 had little influence. These results indicated that (*S*,*S*)-[^{125}I]IPBM selectively accumulated for NET in the heart. Gathering these data, we considered radioiodinated (*S*,*S*)-IPBM to be a more suitable agent for cardiac NET imaging compared with (*R*)-MIPP. In the pharmacological blocking studies, however, about 40% of the radioactivity remained in the heart. Although the cause of this binding is not clear, it is most likely due to high nonspecific binding due to high lipophilicity. This high residual uptake may result in a high background uptake, especially in the denervated heart, and limit the clinical utility of this agent. More studies are required of this high residual uptake.

The uptake in the lung was higher than that in the heart at each point. This may be due to the binding to NET in the lung [21], other binding sites and/or amine metabolic enzymes, such as monoamine oxidase, in the lung [22–24]. It is predicted that a SPECT image will show less accumulation in the lung than the value in biodistribution studies because of the existence of a large amount of air in the lung of a living body. Further imaging studies with (*S*,*S*)-[^{123}I]IPBM may be required.

To compare with MIBG, the heart uptake of (*S*,*S*)-[^{125}I] IPBM was lower than that of [^{125}I]MIBG (Table 3). However, the washout rate (uptake of 15 min/uptake of 180 min) of (*S*,*S*)-[^{125}I]IPBM in the heart was similar to that of [^{125}I]MIBG (IPBM=1.32±0.43 and MIBG=1.32±0.15). Regarding liver uptake, the liver uptake of (*S*,*S*)-[^{125}I]IPBM in 15 and 60 min was lower than that of [^{125}I]MIBG, although both uptakes were similar in 180 min. In other words, the uptake of (*S*,*S*)-[^{125}I]IPBM in the liver was kept in low level. However, the uptake of [^{125}I]MIBG was high level in the early phase, then [^{125}I]MIBG was gradually decreased from the liver. Since high hepatic accumulation is a problem in [^{123}I]MIBG diagnosis [25], this low accumulation of (*S*,*S*)-IPBM in the liver may be an advantage over MIBG. The heart-to-blood ratio (imaging index of heart) of (*S*,*S*)-[^{125}I]IPBM was significantly higher than that of [^{125}I]MIBG. This may also be an advantage of (*S*,*S*)-[^{125}I]IPBM.

In conclusion, (*S*,*S*)-IPBM showed a high affinity and selectivity for NET in vitro and in vivo in the heart. Although further investigation is required, these results indicate that radioiodinated (*S*,*S*)-IPBM is a potential radioligand for NET imaging in the heart.

Acknowledgments

We would like to thank Daiichi Radioisotope Laboratories Ltd., Tokyo, Japan, for providing [^{125}I]MIBG. This study was supported in part by Grants-in-Aid for Scientific Research on Priority Areas (Research on Pathomechanisms of Brain Disorders) from the Ministry of Education, Culture, Sports, Science and Technology of Japan (18023023).

References

[1] Mandela P, Ordway GA. The norepinephrine transporter and its regulation. J Neurochem 2006;97:310–33.

[2] Backs J, Haunstetter A, Gerber SH, Metz J, Borst MM, Strasser RH, et al. The neuronal norepinephrine transporter in experimental heart failure: evidence for a posttranscriptional downregulation. J Mol Cell Cardiol 2001;33:461–72.
[3] Bohm M, La Rosee K, Schwinger RH, Erdmann E. Evidence for reduction of norepinephrine uptake sites in the failing human heart. J Am Coll Cardiol 1995;25:146–53.
[4] Fukumitsu N, Suzuki M, Fukuda T, Kiyono Y, Kajiyama S, Saji H. Reduced ^{125}I-meta-iodobenzylguanidine uptake and norepinephrine transporter density in the hearts of mice with MPTP-induced parkinsonism. Nucl Med Biol 2006;33:37–42.
[5] Kiyono Y, Iida Y, Kawashima H, Ogawa M, Tamaki N, Nishimura H, et al. Norepinephrine transporter density as a causative factor in alterations in MIBG myocardial uptake in NIDDM model rats. Eur J Nucl Med Mol Imaging 2002;29:999–1005.
[6] Shannon JR, Flattem NL, Jordan J, Jacob G, Black BK, Biaggioni I, et al. Orthostatic intolerance and tachycardia associated with norepinephrine-transporter deficiency. N Engl J Med 2000;342:541–9.
[7] Ungerer M, Chlistalla A, Richardt G. Upregulation of cardiac uptake 1 carrier in ischemic and nonischemic rat heart. Circ Res 1996;78: 1037–43.
[8] Keller NR, Diedrich A, Appalsamy M, Tuntrakool S, Lonce S, Finney C, et al. Norepinephrine transporter-deficient mice exhibit excessive tachycardia and elevated blood pressure with wakefulness and activity. Circulation 2004;110:1191–6.
[9] Munch G, Rosport K, Bultmann A, Baumgartner C, Li Z, Laacke L, et al. Cardiac overexpression of the norepinephrine transporter uptake-1 results in marked improvement of heart failure. Circ Res 2005;97:928–36.
[10] Schroeder C, Birkenfeld AL, Mayer AF, Tank J, Diedrich A, Luft FC, et al. Norepinephrine transporter inhibition prevents tilt-induced presyncope. J Am Coll Cardiol 2006;48:516–22.
[11] Carrio I. Cardiac neurotransmission imaging. J Nucl Med 2001;42: 1062–76.
[12] Langer O, Halldin C. PET and SPET tracers for mapping the cardiac nervous system. Eur J Nucl Med Mol Imaging 2002;29:416–34.
[13] Yamashina S, Yamazaki J. Neuronal imaging using SPECT. Eur J Nucl Med Mol Imaging 2007;34:939–50.
[14] Kiyono Y, Kanegawa N, Kawashima H, Fujiwara H, Iida Y, Nishimura H, et al. A new norepinephrine transporter imaging agent for cardiac sympathetic nervous function imaging: radioiodinated (*R*)-*N*-methyl-3-(2-iodophenoxy)-3-phenylpropanamine. Nucl Med Biol 2003;30: 697–706.
[15] Kiyono Y, Kanegawa N, Kawashima H, Kitamura Y, Iida Y, Saji H. Evaluation of radioiodinated (*R*)-*N*-methyl-3-(2-iodophenoxy)-3-phenylpropanamine as a ligand for brain norepinephrine transporter imaging. Nucl Med Biol 2004;31:147–53.
[16] Kanegawa N, Kiyono Y, Kimura H, Sugita T, Kajiyama S, Kawashima H, et al. Synthesis and evaluation of radioiodinated (*S*,*S*)-2-(alpha-(2-iodophenoxy)benzyl)morpholine for imaging brain norepinephrine transporter. Eur J Nucl Med Mol Imaging 2006;33:639–47.
[17] Raisman R, Sette M, Pimoule C, Briley M, Langer SZ. High-affinity [^{3}H]desipramine binding in the peripheral and central nervous system: a specific site associated with the neuronal uptake of noradrenaline. Eur J Pharmacol 1982;78:345–51.
[18] Lowry OH, Rosebrough NJ, Farr AL, Randall RJ. Protein measurements with the Folin phenol reagent. J Biol Chem 1951; 193:265–75.
[19] Haka MS, Kilbourn MR. Synthesis and regional mouse brain distribution of [^{11}C]nisoxetine, a norepinephrine uptake inhibitor. Int J Rad Appl Instrum B 1989;16:771–4.
[20] Nakamura H, Edo K, Hishinuma T, Takahashi T, Ido T, Mizugaki M. Synthesis of ^{11}C-labeled imipramine and its biodistribution in mice: a potential tracer for positron emission tomography. Chem Pharm Bull (Tokyo) 1989;37:3376–9.
[21] Tseng YT, Padbury JF. Expression of a pulmonary endothelial norepinephrine transporter. J Neural Transm 1998;105:1187–91.
[22] Fowler JS, Gallagher BM, MacGregor RR, Wolf AP. Carbon-11 labeled aliphatic amines in lung uptake and metabolism studies: potential for dynamic measurements in vivo. J Pharmacol Exp Ther 1976;198:133–45.
[23] Moretti JL, Zini R, Morin D, Joulin Y, Desplanches G, Caillat-Vigneron N, et al. Interactions of phenylalkylamines with human lung membrane and microsome preparation. Nucl Med Commun 1987;8: 115–20.
[24] Touya JJ, Rahimian J, Grubbs DE, Corbus HF, Bennett LR. A noninvasive procedure for in vivo assay of a lung amine endothelial receptor. J Nucl Med 1985;26:1302–7.
[25] Gill JS, Hunter GJ, Gane G, Camm AJ. Heterogeneity of the human myocardial sympathetic innervation: in vivo demonstration by iodine 123-labeled meta-iodobenzylguanidine scintigraphy. Am Heart J 1993;126:390–8.

BRAIN RESEARCH 1199 (2008) 46-52

available at www.sciencedirect.com

ScienceDirect

www.elsevier.com/locate/brainres

BRAIN RESEARCH

Research Report

5-Iodo-A-85380, a specific ligand for α4β2 nicotinic acetylcholine receptors, prevents glutamate neurotoxicity in rat cortical cultured neurons

Masashi Ueda[a,b], *Yasuhiko Iida*[c], *Youji Kitamura*[d], *Hidekazu Kawashima*[e], *Mikako Ogawa*[f], *Yasuhiro Magata*[f], *Hideo Saji*[b,*]

[a]*Radioisotopes Research Laboratory, Kyoto University Hospital, Faculty of Medicine, Kyoto University, Kyoto 606-8507, Japan*
[b]*Department of Patho-Functional Bioanalysis, Graduate School of Pharmaceutical Sciences, Kyoto University, Kyoto 606-8501, Japan*
[c]*Bioimaging Information Analysis, Graduate School of Medicine, Gunma University, Maebashi, Gunma 371-8512, Japan*
[d]*Graduate School of Medicine and Dentistry and Pharmaceutical Sciences, Okayama University, Okayama 700-8530, Japan*
[e]*Department of Nuclear Medicine and Diagnostic Imaging, Graduate School of Medicine, Kyoto University, Kyoto 606-8507, Japan*
[f]*Laboratory of Genome-Bio Photonics, PhotonMedical Research Center, Hamamatsu University School of Medicine, Hamamatsu, Shizuoka 431-3192, Japan*

ARTICLE INFO

Article history:
Accepted 15 October 2007
Available online 26 January 2008

Keywords:
Nicotinic acetylcholine receptor
α4β2 subtype
5-iodo-A-85380 (5IA)
Neuroprotection
Glutamate toxicity
Extracellular calcium ion

ABSTRACT

5-iodo-3-(2(S)-azetidinylmethoxy)pyridine (5-iodo-A-85380, 5IA) has very high affinity and selectivity to nicotinic acetylcholine receptor (nAChR) α4β2 subtype, and a relative safe profile. To assess whether 5IA has neuroprotective properties, we examined the effect of 5IA on glutamate (Glu)-induced neurotoxicity using primary cultures of rat cortical neurons. A 10-min exposure of cultures to Glu followed by 2-h incubation with drug-free medium caused a marked loss of viability, as determined by trypan blue exclusion method. Glu-induced neurotoxicity was prevented by 5IA both in a time- and concentration-dependent manner. 5IA-induced neuroprotection required pretreatment of 5IA prior to Glu exposure with an optimal concentration of 10 nM and an optimal pretreatment time of 2 h. Treatment after Glu exposure could not rescue the cultured cells. The neuroprotective effect of 5IA was antagonized by mecamylamine, a nAChR antagonist, but not by scopolamine, a muscarinic acetylcholine receptor antagonist. Dihydro-β-erythroidine, an α4β2 nAChR antagonist, completely inhibited 5IA-induced neuroprotection, whereas α-bungarotoxin, an α7 nAChR antagonist, had no effect. Furthermore, 5IA did not show neuroprotective effects in the absence of extracellular Ca^{2+}. These results suggest that the neuroprotective effects of 5IA are produced by activation of α4β2 nAChRs followed by the influx of extracellular Ca^{2+}. In conclusion, 5IA is possibly not only useful for the treatment and prevention of glutamate neurotoxicity, but also as an available tool for elucidating the mechanism of neuroprotection associated with α4β2 nAChRs.

* *Corresponding author*. Department of Patho-Functional Bioanalysis, Graduate School of Pharmaceutical Sciences, Kyoto University, 46-29 Yoshida Shimoadachi-cho, Sakyo-ku, Kyoto 606-8501, Japan. Fax: +81 75 753 4568.
E-mail address: hsaji@pharm.kyoto-u.ac.jp (H. Saji).

Abbreviations: nAChR, nicotinic acetylcholine receptor; 5IA, 5-iodo-3-(2(S)-azetidinylmethoxy)pyridine; Glu, glutamate; MEC, mecamylamine; SCOP, scopolamine; DHβE, dihydro-β-erythroidine; α-BGT, α-bungarotoxin

0006-8993/$ – see front matter © 2008 Elsevier B.V. All rights reserved.
doi:10.1016/j.brainres.2007.10.107

1. Introduction

Nicotinic acetylcholine receptors (nAChRs) are a family of ligand-gated ion channels that regulate neurotransmission in the central and peripheral nervous systems. These receptors are of great interest because they have been implicated in various brain functions, such as cognition, memory and learning (Gotti et al., 1997; Paterson and Nordberg, 2000). In addition, changes in the density of nAChRs have been reported in various neurodegenerative disorders including Alzheimer's disease (Burghaus et al., 2000; O'Brien et al., 2007; Shimohama et al., 1986) and Parkinson's disease (Burghaus et al., 2003; Fujita et al., 2006; Oishi et al., 2007).

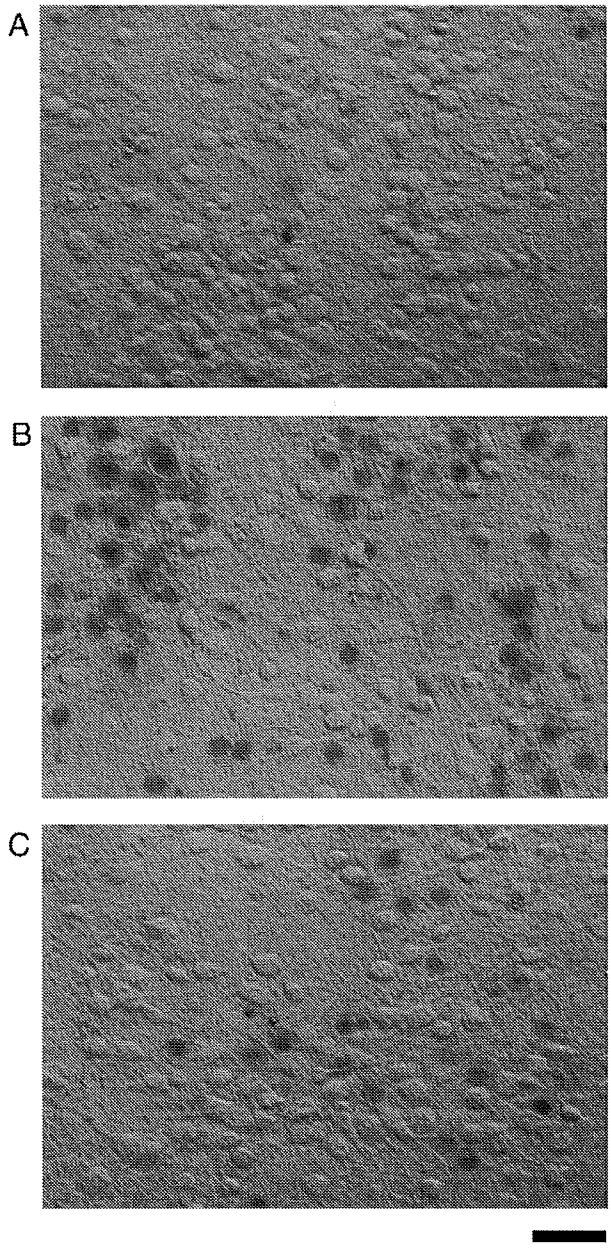

Fig. 1 – Hoffman modulation photomicrographs showing protective effects of 5IA on Glu-induced neurotoxicity. (A) indicates non-treated cells (sham). (B) shows cells treated with 1 mM of Glu for 10 min and further incubated with Glu-free EMEM for 2 h. (C) shows cells exposed to 10 nM of 5IA for 2 h before and during Glu exposure. Calibration bar=50 μm.

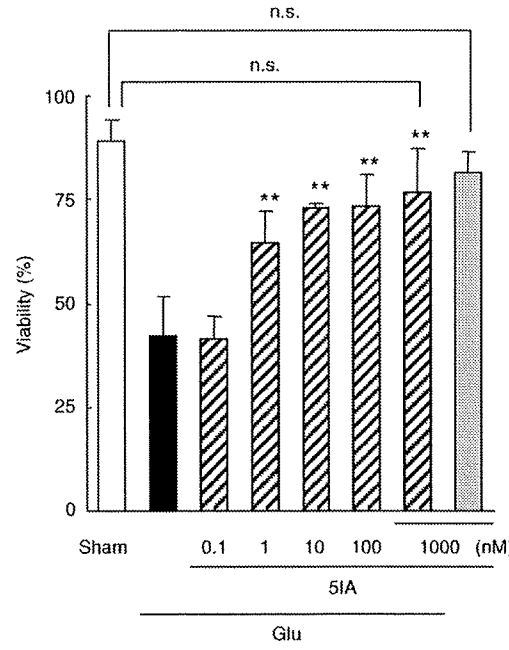

Fig. 2 – Concentration dependency of protective effects of 5IA on acute Glu neurotoxicity. Cultures were treated with 5IA (0.1–1000 nM) for 2 h before and 10 min during Glu exposure, and then incubated with drug-free EMEM for 2 h. **P<0.01, compared with Glu alone. n.s.; not significant. Data represent the means±s.d. of five independent observations.

Neuronal nicotinic receptors are found as pentameric assemblies that can be formed from combinations of at least 11 different receptor subunits (α2–α10 and β2–β4). Although various subtypes are expressed in the mammalian brain, two subtypes of nAChRs, α4β2 and α7, are predominant. Both subtypes have been reported to be involved in the neuroprotective effect against glutamate (Glu)-induced excitatory toxicity (Belluardo et al., 2000). The neuroprotective effects of α7 nAChRs were mediated by the activation of phosphatidylinositol 3-kinase, phosphorylation of Akt and upregulation of the anti-apoptotic protein Bcl-2 (Kihara et al., 2004; Shimohama and Kihara, 2001). On the other hand, the neuroprotective mechanisms of α4β2 nAChRs are still unknown in detail. Since neurotoxicity, mediated by Glu, is thought to play a role in progressive neurodegenerative diseases, such as Alzheimer's disease (Arias et al., 1998; Meldrum and Garthwaite, 1990), α4β2 and α7 nAChR agonists possibly delay the progression of such diseases.

Recently, 5-iodo-3-(2(S)-azetidinylmethoxy)pyridine (5-iodo-A-85380, 5IA), a derivative of A-85380 iodinated at the 5-position of the pyridine ring, was synthesized (Saji et al., 2002). The affinity of 5IA to α4β2 nAChRs was reported to be as high as that of (±)-epibatidine but low for α3β4 nAChRs, responsible for cardiovascular side effects caused by nAChR agonists (Mukhin et al., 2000). 5IA has more selectivity to α4β2 nAChRs than A-85380, the parent compound of 5IA, and in fact, studies have shown a relatively good safety profile for 5IA (Ueda et al., 2004; Vaupel et al., 2003). Thus, it is possible that 5IA will be more useful for the treatment and prevention of neurodegenerative diseases

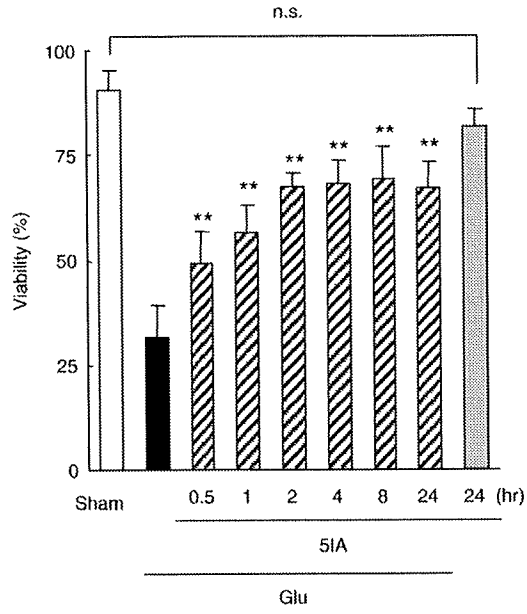

Fig. 3 – Time dependency of protective effects of 5IA on acute Glu neurotoxicity. Cultures were treated with 5IA (10 nM) for 0.5–24 h before and 10 min during Glu exposure, and then incubated with drug-free EMEM for 2 h. **P<0.01, compared with Glu alone. n.s.; not significant. Data represent the means±s.d. of five independent observations.

than other nAChR agonists, such as nicotine. Furthermore, since 5IA has extremely high affinity and selectivity to α4β2 nAChRs, it is suitable to clarify the mechanisms of neuroprotection associated with α4β2 nAChRs.

Therefore, we assessed whether 5IA had neuroprotective properties against Glu-induced neurotoxicity using rat cortical cultures. We also elucidated the nAChR subtype and potential mechanism involved in 5IA-induced neuroprotection.

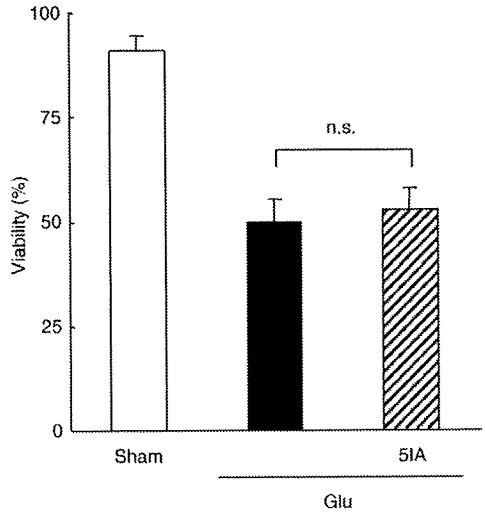

Fig. 4 – Protective effect of 5IA applied after Glu exposure. Cultures were incubated with Glu for 10 min followed by 2-h incubation in EMEM containing 10 nM of 5IA. n.s.; not significant. Data represent the means±s.d. of five independent observations.

2. Results

2.1. *Protective effect of 5IA on glutamate-induced neurotoxicity*

We examined the effect of 5IA on Glu-induced acute neurotoxicity. Fig. 1 shows the typical protective effect of 5IA. Exposure of the cortical cultures to 1 mM of Glu for 10 min markedly increased

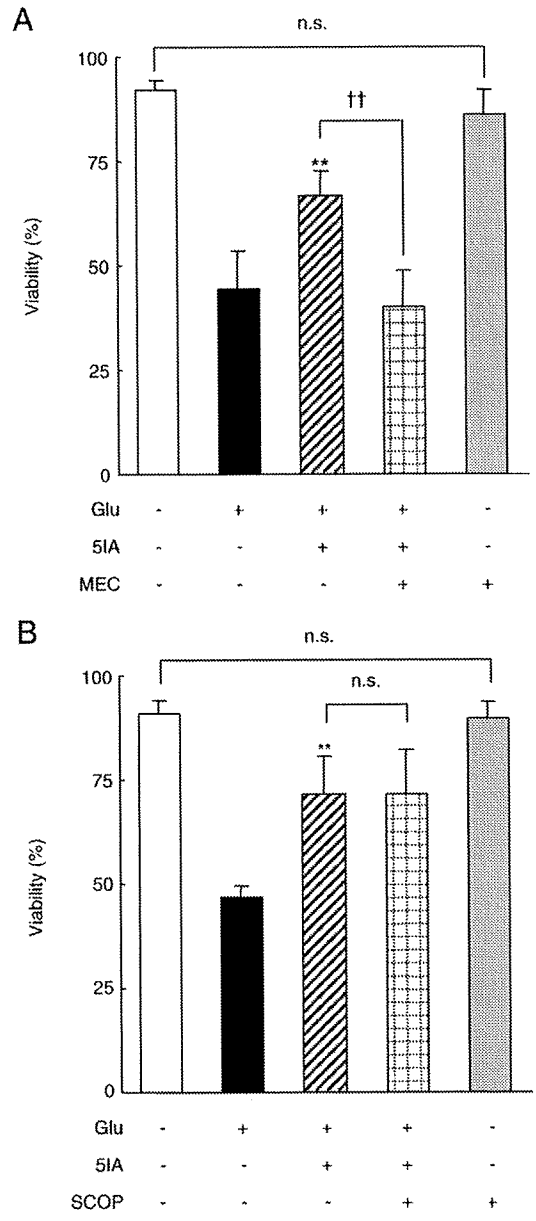

Fig. 5 – Effects of a nicotinic receptor antagonist, mecamylamine (MEC) (A) and a muscarinic receptor antagonist, scopolamine (SCOP) (B) on 5IA-induced neuroprotection against Glu toxicity. Cultures were treated with 5IA and each antagonist (1 μM) for 2 h before and 10 min during Glu exposure, and then incubated with drug-free EMEM for 2 h. **P<0.01, compared with Glu alone. ††P<0.01, compared with 5IA + Glu. n.s.; not significant. Data represent the means±s.d. of five independent observations.

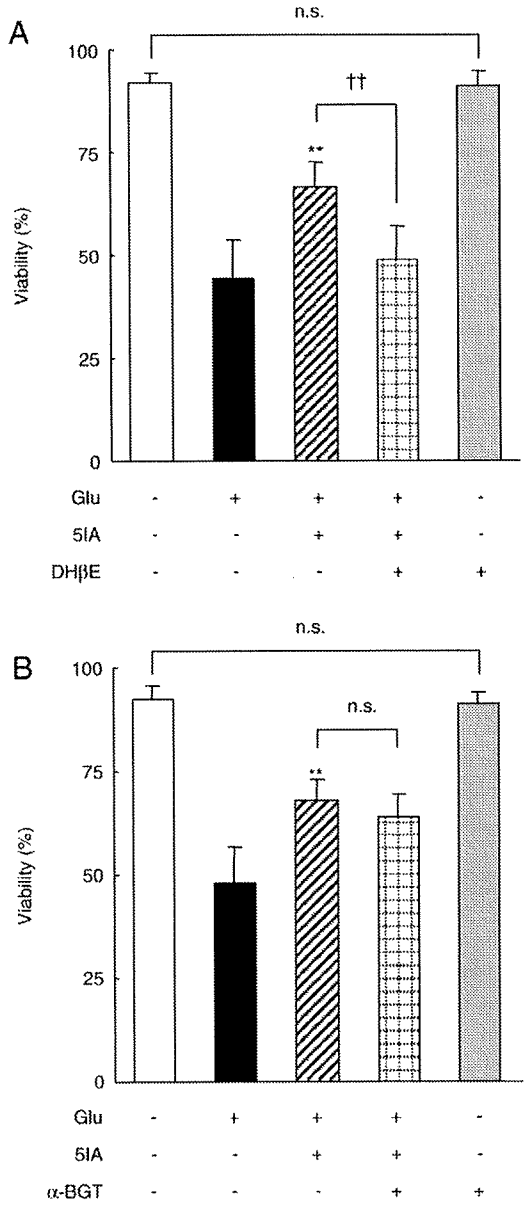

Fig. 6 – Effects of a nAChR α4β2 subtype antagonist, dihydro-β-erythroidine (DHβE) (A) and a nAChR α7 subtype antagonist, α-bungarotoxin (α-BGT) (B) on 5IA-induced neuroprotection against Glu toxicity. Cultures were treated with 5IA and each antagonist (1 μM of DHβE and 1 nM of α-BGT) for 2 h before and 10 min during Glu exposure, and then incubated with drug-free EMEM for 2 h. **P<0.01, compared with Glu alone. ††P<0.01, compared with 5IA + Glu. n.s.; not significant. Data represent the means ± s.d. of five independent observations.

the number of trypan blue-stained cells, i.e., non-viable cells (Fig. 1B). When 5IA was applied, the number of non-viable cells was markedly reduced (Fig. 1C).

Donnelly-Roberts et al. reported that the neuroprotection elicited by ABT-418 and nicotine were time dependent, with an optimal pretreatment time of 2 h (Donnelly-Roberts et al., 1996). Thus, we examined the concentration dependency of the neuroprotective effect of 5IA applied for 2 h prior to Glu exposure. One-tenth nM of 5IA produced no protection against Glu toxicity; however, 1 nM or more of 5IA increased the cell viability significantly. The protective effect reached a plateau at 10 nM (73±1%) (Fig. 2).

Next, the time dependency was investigated. When we applied 10 nM of 5IA for 0.5–24 h prior to Glu exposure, 5IA showed significant protective effects at all pretreatment time points. The protective effect increased dependent on the duration of pretreatment and reached a plateau at 2 h (viability was 67±4%) (Fig. 3).

We also examined the protective effect of 5IA treated after glutamate exposure. When cultures were exposed to Glu for 10 min and subsequently incubated in EMEM containing 10 nM of 5IA for 2 h, no protective effect against Glu toxicity was observed (Glu alone: 50±5%, 5IA: 53±5%) (Fig. 4).

2.2. *Effects of cholinergic antagonists on 5IA-induced neuroprotection*

We examined which subtype of acetylcholine receptor was involved in the neuroprotective effect of 5IA. As shown in Fig. 5, mecamylamine (MEC), a nAChR antagonist, inhibited the neuroprotective effect of 5IA (5IA: 67±6%, 5IA + MEC: 40±9%) and cell viability decreased to the same level as Glu alone (44±10%) (Fig. 5A). On the other hand, scopolamine (SCOP), a muscarinic receptor antagonist, did not affect 5IA-induced neuroprotection at all (5IA: 71 ±9%, 5IA + SCOP: 72±11%) (Fig. 5B).

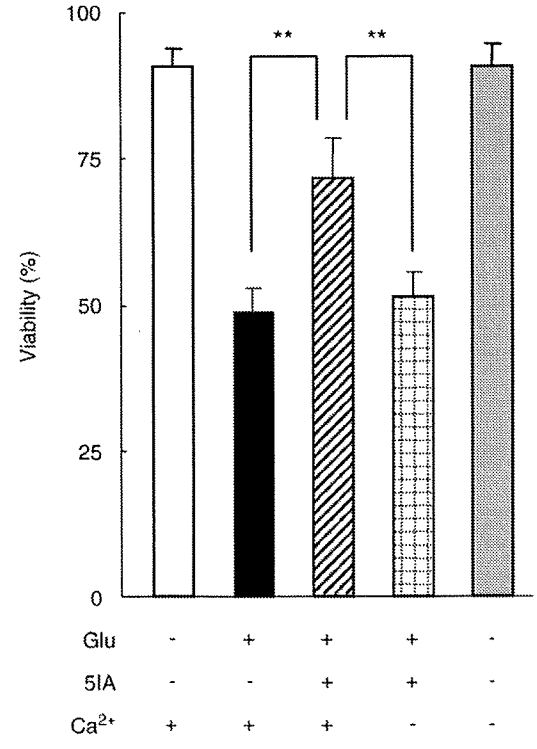

Fig. 7 – Effects of extracellular calcium ions on 5IA-induced neuroprotection against Glu toxicity. Cultures were treated with 5IA in EMEM (including Ca^{2+}) or S-MEM (excluding Ca^{2+}) for 2 h before Glu exposure. 10-min Glu exposure and following 2-h drug-free incubation were performed in EMEM. **P<0.01. Data represent the means ± s.d. of five independent observations.

Furthermore, an α4β2 nAChR antagonist, dihydro-β-erythroidine (DHβE) completely blocked the neuroprotective effect of 5IA (Glu alone: 44±9%, 5IA: 67±6%, 5IA+DHβE: 49±8%) (Fig. 6A), while an α7 nAChR antagonist, α-bungarotoxin (α-BGT) had no effect on 5IA-induced neuroprotection (Glu alone: 48±9%, 5IA: 68±5%, 5IA+α-BGT: 64±6%) (Fig. 6B).

2.3. *Effects of extracellular calcium ion on 5IA-induced neuroprotection*

Finally, we studied the effects of extracellular Ca^{2+} on the protective effect of 5IA against Glu-induced neurotoxicity. Cultures were preincubated with or without 5IA in EMEM (including Ca^{2+}) or S-MEM (Ca^{2+}-free EMEM) for 2 h, and then 10-min Glu exposure and 2-h drug-free incubation were performed in EMEM. As shown in Fig. 7, although the pretreatment of 5IA in Ca^{2+}-including medium attenuated Glu-induced neurotoxicity, pretreatment in Ca^{2+}-free medium could not block toxicity (Glu alone: 49±4%, 5IA with Ca^{2+}: 72±7%, 5IA without Ca^{2+}: 51±4%). The cultures incubated in Ca^{2+}-free medium maintained high viability under Glu-free conditions (91±4%) (Fig. 7).

3. Discussion

In the present study, we investigated the effects of 5IA on Glu-induced neurotoxicity using primary cultures of rat cortical neurons. 5IA prevented Glu-induced neurotoxicity both in a time- and concentration-dependent manner. 5IA-induced neuroprotection required pretreatment of 5IA prior to Glu exposure. Treatment after Glu exposure could not rescue the cultured cells. These results are consistent with previous reports that investigated the neuroprotective effects of other nAChR agonists against Glu-mediated toxicity (Akaike et al., 1994; Donnelly-Roberts et al., 1996; Shimohama et al., 1996), although the concentration of nAChR agonists used was quite different. In our study, 10 nM of 5IA showed comparable neuroprotective effects to previous reports in which 10 μM of nicotine or ABT-418 was used. Moreover, in an FLIPR assay using HEK-293 cells stably expressing human α4β2 nAChRs, 5IA showed about 50 times higher EC_{50} values than TC-2559 (Zwart et al., 2006), which showed similar efficacy and potency to nicotine and ABT-418 on Rb^+ release from rat thalamic synaptosomes (Bencherif et al., 2000). These results indicate that 5IA has much higher efficacy and potency on α4β2 nAChRs than other nAChR agonists.

Next, we examined which subtype of acetylcholine receptor was involved in the neuroprotective effect of 5IA using nicotinic and muscarinic antagonists. As expected, mecamylamine antagonized the effect of 5IA completely but scopolamine did not. Moreover, DHβE also blocked 5IA-induced neuroprotection completely, while α-BGT had no effect. This result suggests that the neuroprotective effect of 5IA is mediated only by α4β2 nAChRs and that neither α7 nAChRs nor muscarinic acetylcholine receptors are involved in the effect of 5IA. This result is in contrast to many studies that have reported neuroprotection evoked by nAChR stimulation against Glu-induced cytotoxicity mediated, at least in part, by α7 nAChRs (Akaike et al., 1994; Donnelly-Roberts et al., 1996; Kaneko et al., 1997; Takada et al., 2003). Muhkin et al. reported that the α7/α4β2 ratio calculated from the Ki value of 5IA was 25,000, whereas that of nicotine was only 170 (Mukhin et al., 2000); that is to say, 5IA had approximately 150 times greater selectivity for α4β2 nAChRs than nicotine. Because of this selectivity, it is likely that 5IA, at the low concentration used in this study, acted almost entirely on α4β2 nAChRs. This suggests that 5IA could be useful to elucidate the mechanism of α4β2 nAChR-mediated neuroprotection.

Although excessive influx of Ca^{2+} causes neuronal death, increases of intracellular Ca^{2+} can trigger the activation of Ca^{2+}-dependent protein kinases involved in neuroprotective cell signaling. α4β2 nAChRs are reported to be to Ca^{2+}-permeable although less so than α7 nAChRs (Jensen et al., 2005). Moreover, they are permeable to monovalent cations and the influx of Na^+ could depolarize the cell thereby activating voltage-gated Ca^{2+} channels (VGCCs) and increase Ca^{2+} entry (Nakayama et al., 2001). Consequently, we investigated the effect of extracellular Ca^{2+} on 5IA-mediated neuroprotective action. As shown in Fig. 7, the protective effect of 5IA was diminished by removing extracellular Ca^{2+}. This result demonstrates that extracellular Ca^{2+} plays a critical role in neuroprotection mediated not only by α7 nAChRs (Donnelly-Roberts et al., 1996) but also by α4β2 nAChRs. In fact, Dickinson et al. have recently demonstrated that the primary route of Ca^{2+} entry following 5IA treatment is via L-type VGCC and that the resulting increases of intracellular Ca^{2+} were α-BGT-insensitive (Dickinson et al., 2007). Thus, the influx of Ca^{2+} through α4β2 nAChRs and/or through VGCCs induced by the activation of α4β2 nAChRs could play a role in the neuroprotective action of 5IA.

Further mechanisms underlying 5IA-induced neuroprotection have not yet been elucidated. The activation of Ca^{2+}/calmodulin-dependent protein kinase II (CaMKII), phosphatidylinositol 3-kinase (PI3-K) and the downstream PI3-K target Akt have been reported to be important in the calcium-mediated promotion of survival in neurons (Ikegami and Koike, 2000). Vaillant et al. reported that Ca^{2+} influx via VGCCs was involved in activation of the CaMKII pathway and Ras–PI3-K–Akt pathway (Vaillant et al., 1999); therefore, 5IA-induced neuroprotection potentially occurs through both of these pathways.

Neurotrophic factors may also be involved in 5IA-induced neuroprotection. It was reported that ABT-594, an analogue of 5IA, increased fibroblast growth factor-2 (FGF-2) mRNA levels (Belluardo et al., 1999) and that FGF-2 protected cultured neurons from NMDA-mediated excitotoxicity (Freese et al., 1992). Moreover, Roceri et al. reported that the expression of FGF-2 was regulated in a Ca^{2+}-dependent manner (Roceri et al., 2000). Thus, it is possible that 5IA shows neuroprotective effects by affecting the expression of FGF-2.

In summary, we have revealed that 5IA has neuroprotective effects against Glu-induced cytotoxicity at a much lower concentration than other nAChR agonists. These effects required the treatment of 5IA prior to Glu exposure and were mediated not by α7 nAChRs but by α4β2 nAChRs. Moreover, extracellular Ca^{2+} was essential for 5IA-induced neuroprotection. These findings suggest that the neuroprotective effects of 5IA are produced by the activation of α4β2 nAChRs followed by the influx of extracellular Ca^{2+}. In conclusion, 5IA is possibly more useful for the treatment and prevention of neurodegenerative diseases than other nAChR agonists because of its high efficacy and selectivity, and should be a valuable tool for elucidating the mechanism of neuroprotection associated with α4β2 nAChRs.

4. Experimental procedures

4.1. Materials

Eagle's minimal essential salt medium (EMEM) was purchased from Nissui Pharmaceutical (Tokyo, Japan). Ca^{2+}-free EMEM (S-MEM) was purchased from Invitrogen (Carlsbad, CA). Fetal bovine serum and horse serum were purchased from JRH Biosciences (Lenexa, KS) and Invitrogen, respectively. Drugs were obtained from the following sources: D-(+)-glucose, sodium hydrogen carbonate ($NaHCO_3$), HEPES, L-glutamic acid monosodium salt and trypan blue (Nacalai Tesque, Kyoto, Japan), cytosine-1-β-D(+)-arabinofuranoside (Ara-C) (Wako Pure Chemical Industries, Osaka, Japan), L-glutamine, mecamylamine hydrochloride and dihydro-β-erythroidine hydrobromide (Sigma-Aldrich, St. Louis, MO), (–)-scopolamine hydrobromide (RBI, Natick, MA), α-bungarotoxin and ionomycin (EMD Biosciences, San Diego, CA). 5IA was synthesized according to the previously published methods (Saji et al., 2002).

4.2. Cell culture

Animals were treated in accordance with the guidelines of the Kyoto University Animal Care Committee.

Primary cultures were obtained from the cerebral cortex of fetal rats (17–18 days of gestation) using a modified method described previously (Takada-Takatori et al., 2006) with a slight modification. Briefly, single cells dissociated from the whole cerebral cortex of fetal rats were plated on plastic coverslips attached in 60 mm dishes (4.5×10^6 cells per dish). Cultures were incubated in EMEM supplemented with 5% heat-inactivated fetal bovine serum and 5% heat-inactivated horse serum (1–7 days after plating) or 5% heat-inactivated horse serum (8–12 days after plating), L-glutamine (2 mM), D-(+)-glucose (11 mM), $NaHCO_3$ (24 mM) and HEPES (10 mM). Cultures were maintained at 37 °C in a humidified 5% CO_2 atmosphere. After 6 days of plating, non-neuronal cells were removed by the addition of Ara-C (10 μM). Only mature cultures (11–12 days in vitro) were used for experiments.

4.3. Drug treatment

Exposure to Glu (1 mM) was carried out in EMEM. The cultures were exposed to Glu for 10 min and then incubated in drug-free EMEM for 2 h. Unless otherwise indicated, 5IA was applied for 2 h before and 10 min during Glu exposure. Cholinergic antagonists (MEC, SCOP, DHβE and α-BGT) were added to EMEM concomitant with 5IA. All experiments were performed at 37 °C.

4.4. Measurement of neurotoxicity

Neurotoxicity induced by Glu was quantitatively assessed by examining cultures under Hoffman modulation microscopy as described previously (Kitamura et al., 2006; Taguchi et al., 2003) with a slight modification. Cell viability was assessed by the trypan blue exclusion method, i.e., cell cultures were stained with 1.5% trypan blue solution for 3 min at room temperature and then rinsed with physiological saline. The stained cells were regarded as non-viable. In each experiment, cells on five coverslips were counted to obtain the means±s.d. of cell viability.

4.5. Statistics

Data are expressed as the means±s.d. The statistical significance of difference between groups was determined by one-way analysis of variance (ANOVA) followed by Tukey–Kramer multiple comparison tests. Differences were considered significant when $p<0.05$.

Acknowledgments

We thank Professor Akinori Akaike and his laboratory members (Department of Pharmacology, Graduate School of Pharmaceutical Sciences, Kyoto University) for their technical support and invaluable discussions on the cell culture and neurotoxicity assays. This work was supported in part by a grant-in-aid for Scientific Research from the Ministry of Education, Science and Technology of Japan and a grant from the Smoking Research Foundation.

REFERENCES

Akaike, A., Tamura, Y., Yokota, T., Shimohama, S., Kimura, J., 1994. Nicotine-induced protection of cultured cortical neurons against N-methyl-D-aspartate receptor-mediated glutamate cytotoxicity. Brain Res. 644, 181–187.

Arias, C., Becerra-Garcia, F., Tapia, R., 1998. Glutamic acid and Alzheimer's disease. Neurobiology. (Bp). 6, 33–43.

Belluardo, N., Mudo, G., Caniglia, G., Cheng, Q., Blum, M., Fuxe, K., 1999. The nicotinic acetylcholine receptor agonist ABT-594 increases FGF-2 expression in various rat brain regions. Neuroreport 10, 3909–3913.

Belluardo, N., Mudo, G., Blum, M., Fuxe, K., 2000. Central nicotinic receptors, neurotrophic factors and neuroprotection. Behav. Brain Res. 113, 21–34.

Bencherif, M., Bane, A.J., Miller, C.H., Dull, G.M., Gatto, G.J., 2000. TC-2559: a novel orally active ligand selective at neuronal acetylcholine receptors. Eur. J. Pharmacol. 409, 45–55.

Burghaus, L., Schutz, U., Krempel, U., de Vos, R.A., Jansen Steur, E.N., Wevers, A., Lindstrom, J., Schroder, H., 2000. Quantitative assessment of nicotinic acetylcholine receptor proteins in the cerebral cortex of Alzheimer patients. Brain Res. Mol. Brain Res. 76, 385–388.

Burghaus, L., Schutz, U., Krempel, U., Lindstrom, J., Schroder, H., 2003. Loss of nicotinic acetylcholine receptor subunits alpha4 and alpha7 in the cerebral cortex of Parkinson patients. Parkinsonism Relat. Disord. 9, 243–246.

Dickinson, J.A., Hanrott, K.E., Mok, M.H., Kew, J.N., Wonnacott, S., 2007. Differential coupling of alpha7 and non-alpha7 nicotinic acetylcholine receptors to calcium-induced calcium release and voltage-operated calcium channels in PC12 cells. J. Neurochem. 100, 1089–1096.

Donnelly-Roberts, D.L., Xue, I.C., Arneric, S.P., Sullivan, J.P., 1996. In vitro neuroprotective properties of the novel cholinergic channel activator (ChCA), ABT-418. Brain Res. 719, 36–44.

Freese, A., Finklestein, S.P., DiFiglia, M., 1992. Basic fibroblast growth factor protects striatal neurons in vitro from NMDA-receptor mediated excitotoxicity. Brain Res. 575, 351–355.

Fujita, M., Ichise, M., Zoghbi, S.S., Liow, J.S., Ghose, S., Vines, D.C., Sangare, J., Lu, J.Q., Cropley, V.L., Iida, H., Kim, K.M., Cohen, R.M., Bara-Jimenez, W., Ravina, B., Innis, R.B., 2006. Widespread decrease of nicotinic acetylcholine receptors in Parkinson's disease. Ann. Neurol. 59, 174–177.

Gotti, C., Fornasari, D., Clementi, F., 1997. Human neuronal nicotinic receptors. Prog. Neurobiol. 53, 199–237.

Ikegami, K., Koike, T., 2000. Membrane depolarization-mediated survival of sympathetic neurons occurs through both phosphatidylinositol 3-kinase- and CaM kinase II-dependent pathways. Brain Res. 866, 218–226.

Jensen, A.A., Frolund, B., Liljefors, T., Krogsgaard-Larsen, P., 2005. Neuronal nicotinic acetylcholine receptors: structural revelations, target identifications, and therapeutic inspirations. J. Med. Chem. 48, 4705–4745.

Kaneko, S., Maeda, T., Kume, T., Kochiyama, H., Akaike, A., Shimohama, S., Kimura, J., 1997. Nicotine protects cultured cortical neurons against glutamate-induced cytotoxicity via alpha7-neuronal receptors and neuronal CNS receptors. Brain Res. 765, 135–140.

Kihara, T., Sawada, H., Nakamizo, T., Kanki, R., Yamashita, H., Maelicke, A., Shimohama, S., 2004. Galantamine modulates nicotinic receptor and blocks Abeta-enhanced glutamate toxicity. Biochem. Biophys. Res. Commun. 325, 976–982.

Kitamura, Y., Iida, Y., Abe, J., Ueda, M., Mifune, M., Kasuya, F., Ohta, M., Igarashi, K., Saito, Y., Saji, H., 2006. Protective effect of zinc against ischemic neuronal injury in a middle cerebral artery occlusion model. J. Pharmacol. Sci. 100, 142–148.

Meldrum, B., Garthwaite, J., 1990. Excitatory amino acid neurotoxicity and neurodegenerative disease. Trends Pharmacol. Sci. 11, 379–387.

Mukhin, A.G., Gundisch, D., Horti, A.G., Koren, A.O., Tamagnan, G., Kimes, A.S., Chambers, J., Vaupel, D.B., King, S.L., Picciotto, M.R., Innis, R.B., London, E.D., 2000. 5-Iodo-A-85380, an alpha4beta2 subtype-selective ligand for nicotinic acetylcholine receptors. Mol. Pharmacol. 57, 642–669.

Nakayama, H., Numakawa, T., Ikeuchi, T., Hatanaka, H., 2001. Nicotine-induced phosphorylation of extracellular signal-regulated protein kinase and CREB in PC12h cells. J. Neurochem. 79, 489–498.

O'Brien, J.T., Colloby, S.J., Pakrasi, S., Perry, E.K., Pimlott, S.L., Wyper, D.J., McKeith, I.G., Williams, E.D., 2007. Alpha4beta2 nicotinic receptor status in Alzheimer's disease using 123I-5IA-85380 single-photon-emission computed tomography. J. Neurol. Neurosurg. Psychiatry 78, 356–362.

Oishi, N., Hashikawa, K., Yoshida, H., Ishizu, K., Ueda, M., Kawashima, H., Saji, H., Fukuyama, H., 2007. Quantification of nicotinic acetylcholine receptors in Parkinson's disease with (123)I-5IA SPECT. J. Neurol. Sci. 256, 52–60.

Paterson, D., Nordberg, A., 2000. Neuronal nicotinic receptors in the human brain. Prog. Neurobiol. 61, 75–111.

Roceri, M., Molteni, R., Racagni, G., Riva, M.A., 2000. Calcium-dependent modulation of FGF-2 expression in cultured cerebellar granule neurons. Neuroreport 11, 3615–3619.

Saji, H., Ogawa, M., Ueda, M., Iida, Y., Magata, Y., Tominaga, A., Kawashima, H., Kitamura, Y., Nakagawa, M., Kiyono, Y., Mukai, T., 2002. Evaluation of radioiodinated 5-iodo-3-(2(S)-azetidinylmethoxy)pyridine as a ligand for SPECT investigations of brain nicotinic acetylcholine receptors. Ann. Nucl. Med. 16, 189–200.

Shimohama, S., Kihara, T., 2001. Nicotinic receptor-mediated protection against beta-amyloid neurotoxicity. Biol. Psychiatry 49, 233–239.

Shimohama, S., Taniguchi, T., Fujiwara, M., Kameyama, M., 1986. Changes in nicotinic and muscarinic cholinergic receptors in Alzheimer-type dementia. J. Neurochem. 46, 288–293.

Shimohama, S., Akaike, A., Kimura, J., 1996. Nicotine-induced protection against glutamate cytotoxicity. Nicotinic cholinergic receptor-mediated inhibition of nitric oxide formation. Ann. N.Y. Acad. Sci. 356–361.

Taguchi, R., Nishikawa, H., Kume, T., Terauchi, T., Kaneko, S., Katsuki, H., Yonaga, M., Sugimoto, H., Akaike, A., 2003. Serofendic acid prevents acute glutamate neurotoxicity in cultured cortical neurons. Eur. J. Pharmacol. 477, 195–203.

Takada, Y., Yonezawa, A., Kume, T., Katsuki, H., Kaneko, S., Sugimoto, H., Akaike, A., 2003. Nicotinic acetylcholine receptor-mediated neuroprotection by donepezil against glutamate neurotoxicity in rat cortical neurons. J. Pharmacol. Exp. Ther. 306, 772–777.

Takada-Takatori, Y., Kume, T., Sugimoto, M., Katsuki, H., Sugimoto, H., Akaike, A., 2006. Acetylcholinesterase inhibitors used in treatment of Alzheimer's disease prevent glutamate neurotoxicity via nicotinic acetylcholine receptors and phosphatidylinositol 3-kinase cascade. Neuropharmacology 51, 474–486.

Ueda, M., Iida, Y., Mukai, T., Mamede, M., Ishizu, K., Ogawa, M., Magata, Y., Konishi, J., Saji, H., 2004. 5-[123I]Iodo-A-85380: assessment of pharmacological safety, radiation dosimetry and SPECT imaging of brain nicotinic receptors in healthy human subjects. Ann. Nucl. Med. 18, 337–344.

Vaillant, A.R., Mazzoni, I., Tudan, C., Boudreau, M., Kaplan, D.R., Miller, F.D., 1999. Depolarization and neurotrophins converge on the phosphatidylinositol 3-kinase-Akt pathway to synergistically regulate neuronal survival. J. Cell Biol. 146, 955–966.

Vaupel, D.B., Tella, S.R., Huso, D.L., Mukhin, A.G., Baum, I., Wagner, V.O., Horti, A.G., London, E.D., Koren, A.O., Kimes, A.S., 2003. Pharmacology, toxicology, and radiation dosimetry evaluation of [I-123]5-I-a-85380, a radioligand for in vivo imaging of cerebral neuronal nicotinic acetylcholine receptors in humans. Drug Dev. Res. 58, 149–168.

Zwart, R., Broad, L.M., Xi, Q., Lee, M., Moroni, M., Bermudez, I., Sher, E., 2006. 5-I A-85380 and TC-2559 differentially activate heterologously expressed alpha4beta2 nicotinic receptors. Eur. J. Pharmacol. 539, 10–17.